Turbulent fluxes and transfer of trace gases from ship-based measurements during TexAQS 2006

Andrey A. Grachev,[1,2] Ludovic Bariteau,[1,2] Christopher W. Fairall,[1] Jeffrey E. Hare,[1,2] Detlev Helmig,[3] Jacques Hueber,[3] and E. Kathrin Lang[3]

Received 13 December 2010; revised 15 March 2011; accepted 14 April 2011; published 13 July 2011.

[1] Air-sea/land turbulent fluxes of momentum, sensible heat, water vapor, carbon dioxide, and ozone are discussed on the basis of eddy covariance measurements made aboard the NOAA R/V *Ronald H. Brown* during the Texas Air Quality Study (TexAQS) in August–September 2006. The TexAQS 2006 field campaign focused on air pollution meteorology associated primarily with ozone and aerosol transport in the Houston/Galveston region and the nearby coastal zone. The ship-based complement of instrumentation was used for the boundary layer measurements over water (the Gulf of Mexico and various harbors/bay areas) and "over land" (specifically, 80 km inside the Houston Ship Channel). In this study we focus on direct comparisons of TexAQS 2006 flux observations with the Coupled Ocean-Atmosphere Response Experiment (COARE) bulk flux algorithm to investigate possible coastal and urban area influences. It is found that the average neutral drag coefficient can be about an order of magnitude larger over very rough urban areas than over the sea surface. However, a similar effect was not observed for the scalar transfer; that is, the neutral Stanton and Dalton numbers do not change significantly over different footprint surfaces. Our data suggest that the TexAQS 2006 region was generally a sink for surface ozone whether over water or over land. The turbulent flux of carbon dioxide was mostly negative (uptake by the surface) for measurements over waters of the Gulf of Mexico and some bays, but the flux becomes positive (release to the air) for inland regions. Both ozone and carbon dioxide turbulent fluxes above land were larger in magnitude compared to the over water measurements.

Citation: Grachev, A. A., L. Bariteau, C. W. Fairall, J. E. Hare, D. Helmig, J. Hueber, and E. K. Lang (2011), Turbulent fluxes and transfer of trace gases from ship-based measurements during TexAQS 2006, *J. Geophys. Res.*, *116*, D13110, doi:10.1029/2010JD015502.

1. Introduction

[2] In August and September 2006, the major multi-institutional intensive field operations of the Texas Air Quality Study (TexAQS) and the Gulf of Mexico Atmospheric Composition and Climate Study (GoMACCS) were conducted. The joint TexAQS/GoMACCS field campaign addressed air quality issues in the northwestern Gulf of Mexico and southeastern Texas. The research program focused on the study of sources, sinks, and transport of trace gases (primarily ozone) and aerosols in the atmosphere and on the influence that these species have on radiative forcing of climate regionally and globally. Field operations included measurements from several satellites and aircraft, the NOAA R/V *Ronald H. Brown*, and ground-based measurements.

[3] The R/V *Ronald H. Brown* provided meteorological and chemical sampling off the coast of Texas including the harbors and bay areas of Galveston, Beaumont, Port Arthur, Freeport, and Matagorda, and in the Houston metropolitan area along the Houston Ship Channel [*Bates et al.*, 2008]. Houston is the fourth largest city in the USA, and the Port of Houston is one of the busiest U.S. sea ports. The petrochemical complex associated with the Port of Houston is one of the largest in the world. The measurements from the ship permit a relative assessment of the contribution of the urban, industrial and shipping emissions from these areas to the regional air pollution and aerosol loading. The near-surface concentrations of pollutant gases and aerosols results from a complicated balance of sources, sinks, chemical reactions, aerosol dynamics, advection, and turbulent transport. Surface energy and turbulent fluxes are the basic driving forces for the atmospheric boundary layer (ABL) development, transporting and mixing trace gases near the surface, and fundamental parameters used for model validation are obtained in the ABL. This includes ABL depth, wind profiles, entrainment velocity/fluxes at the top of the ABL, and other parameters that are also important vari-

[1]NOAA Earth System Research Laboratory, Boulder, Colorado, USA.
[2]Cooperative Institute for Research in Environmental Sciences, University of Colorado at Boulder, Boulder, Colorado, USA.
[3]Institute of Alpine and Arctic Research, University of Colorado at Boulder, Boulder, Colorado, USA.

0148-0227/11/2010JD015502

ables for gaseous/aerosol properties as well as for the ABL dynamics.

[4] Instruments on the R/V *Ronald H. Brown* provided continuous direct measurements of the turbulent fluxes of momentum, heat, moisture, and trace gases by several different methods. A sonic anemometer/thermometer and a high-speed infrared H_2O/CO_2 sensor were used to make measurements of the turbulent fluxes. The flux instrument package also provided accurate measurements of the standard meteorological and ABL parameters. Radar profiler data have been used to determine the ABL height and the wind and temperature structure in and above the ABL. Radiosondes, launched several times a day, measured atmospheric wind, temperature, and moisture profiles. An onboard ceilometer provided the height of the cloud base.

[5] While progress has been made in studying turbulent air-sea fluxes of momentum, heat, and water vapor [e.g., *Fairall et al.*, 2003], an equivalent understanding of the transfer of trace gases over oceans (carbon dioxide, ozone, etc.), does not exist. During the past few years, systems with open-path and closed-path gas analyzers for direct measurements of carbon dioxide fluxes have been deployed in different regions of the world's oceans [*McGillis et al.*, 2001a, 2001b, 2004; *Hare et al.*, 2004]. The measurement of direct covariance ozone (O_3) fluxes over oceans is a recent breakthrough, and during the TexAQS 2006 cruise, an ozone analyzer was added to the NOAA/ESRL flux system [*Bariteau et al.*, 2010].

[6] The purpose of this study is to examine and provide quantitative descriptions of surface exchange fluxes and how these impact the atmospheric sources and sinks of gases in the different pollution source regions; for example, in the coastal waters of the Gulf of Mexico, in the harbors and bay areas, and in the Houston urban area along the ship channel. The analysis presented herein emphasizes the mean transfer coefficients and comparisons of the flux observations with the COARE bulk algorithm [*Fairall et al.*, 2003] to investigate coastal influences on the fluxes. TexAQS 2006 was principally a pollution experiment and therefore a separate focus of the study is associated with direct measurements of the carbon dioxide and ozone turbulent fluxes under different conditions.

2. Measurements and Instrumentation

[7] The NOAA's Earth System Research Laboratory (ESRL) Physical Science Division (formerly the Environmental Technology Laboratory (ETL)) flux group has spent two decades developing techniques for accurate ship-based measurements of direct turbulent energy and gas fluxes. Flux measurements are accompanied by standard meteorological measurements and boundary layer soundings. The open ocean observations form the basis of version 3.0 of the COARE bulk flux algorithm [*Fairall et al.*, 2003]. Overviews of the NOAA ETL/ESRL sea-going measurement systems are provided by *Fairall et al.* [1997, 2006]. Thus, only the relevant information about the TexAQS 2006 cruise instruments and flux data will be given here.

[8] Flux measurements on board the R/V *Ronald H. Brown* were taken from 27 July to 11 September 2006 (year days (YD) = 208–254). However, in this study only the data beginning with YD = 214, when the ship arrived on the Galveston beam, were considered. The data were collected in the northwestern coastal zone of the Gulf of Mexico, in industrialized harbor areas along the Texas coastline, and in the Houston Ship Channel (Figure 1). The cruise track included passages into Port Arthur/Beaumont, Matagorda Bay, Freeport Harbor, Galveston Bay to Barbour's cut (15 transits), and the Houston Ship Channel (4 transits). Satellite images of this region obtained during TexAQS 2006 are provided by *Langford et al.* [2010]. Spatial distribution of dominant land-use types around the Houston-Galveston Bay area is provided by *Lee et al.* [2011, Figure 2]. More information on the ship track and an overview of the other ship activities and results is given by *Bates et al.* [2008], *Day et al.* [2010], *Langford et al.* [2010], *Lee et al.* [2011], and *Tucker et al.* [2010].

[9] Three components of the wind velocity vector and the sonic temperature were measured with a sonic anemometer/thermometer with full motion corrections. In the TexAQS 2006 field campaign a three-axis ultrasonic anemometer/thermometer Gill/IN USA R3A and integrated package of angular rate sensors and accelerometers (Systron Donner Motionpak) for platform motion corrections were used. A high-speed infrared hygrometer Licor-7500 was used for direct measurements of water vapor and carbon dioxide (Figure 2). The flux system was mounted on the ship jackstaff, 18 m above the mean sea surface. Sonic temperature was corrected for velocity crosstalk and the humidity contribution, as discussed by *Fairall et al.* [1997]. Several data quality control criteria have been applied to the original flux data. Flux data have been edited for unfavorable relative wind directions, mean wind vector tilt, maneuvering of the ship during the record, contamination of the turbulence data by the ship's wake, precipitation, and salt contamination (see *Edson et al.* [1998] and *Fairall et al.* [1997, 2003] for details). On the basis of established criteria, the best flux estimates have been used.

[10] During TexAQS 2006, a fast response chemiluminescence instrument for measurements of the ozone deposition flux was deployed for the first time aboard a ship. This instrument was previously operated at the Ameriflux Tower in Niwot Ridge (Colorado) during the summer of 2002. The physical components and installation on a ship platform are illustrated in Figures 2 and 3. The ozone measurement technique is based on the ozone-nitric oxide chemiluminescence reaction

$$NO + O_3 \rightarrow NO_2 + O_2 + \text{photon}$$

and counting of photons resulting from the reaction. This measurement approach has been proven to be the most sensitive technique for eddy-correlation ozone flux measurements [*Bariteau et al.*, 2010].

[11] Ozone was monitored continuously by sampling air through 30 m long Teflon sampling line (Figure 3) to the fast ozone sensor deployed on the third ship deck. The sampling inlet with a fine inlet filter (5 μm) was located on the bow tower, near the sonic anemometer (Figure 2). From the inlet two tubes were running to an UV-O3 instrument, Monitor Lab 8810 and the fast response chemiluminescence monitor. The Monitor Lab 8810 was calibrated against a TEI 49C Ozone Analyzer which was referenced against an

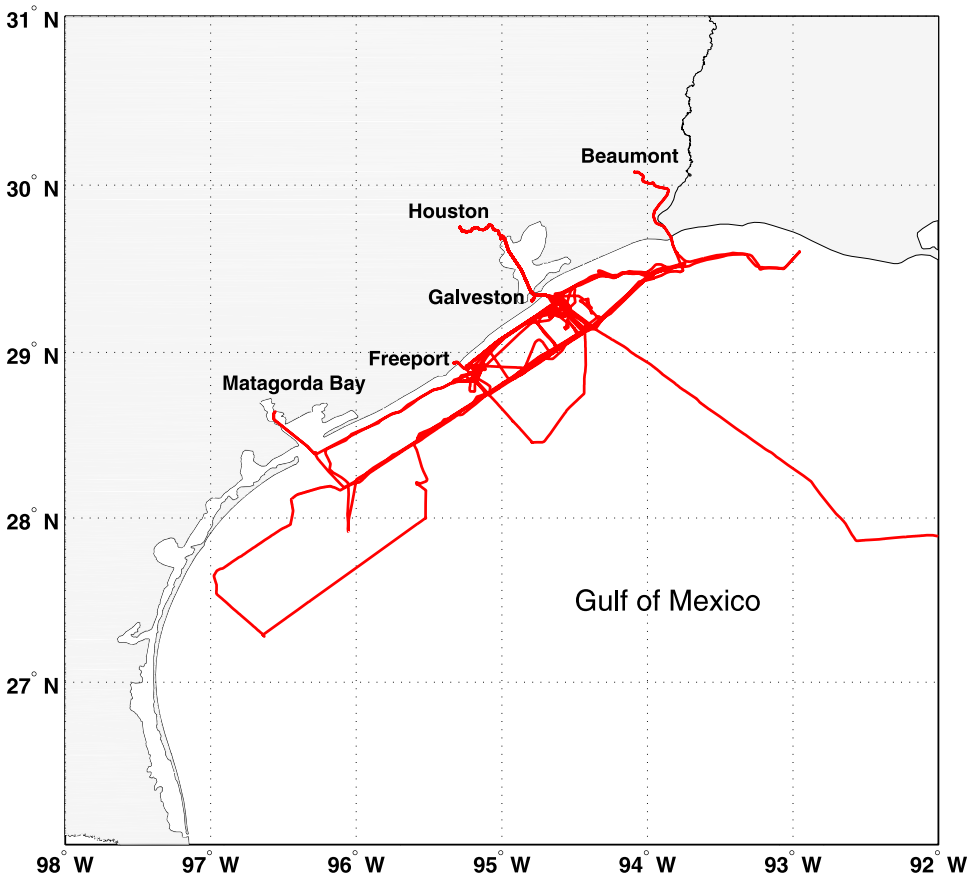

Figure 1. R/V *Ronald H. Brown* cruise track during TexAQS 2006.

EPA standard. Other details of these ozone flux measurements are discussed by *Bariteau et al.* [2010].

[12] Vertical turbulent fluxes of momentum, sensible heat, water vapor, carbon dioxide, and ozone are based on the correlation of the appropriate signals from the different sensors with the vertical component of the wind speed vector measured by a sonic anemometer (eddy correlation method). All turbulent data were sampled at 10 Hz rate. As mentioned above, the measurement of the wind velocity on a seagoing ship is contaminated by a platform motion. Ship motion corrections are applied to the high-frequency sonic anemometer signals prior to computation of the turbulent fluxes, and flow distortion corrections were routinely applied to the final flux results. Details of the motion correction are provided by *Edson et al.* [1998]. A correction term was applied to the computed water vapor, carbon dioxide, and ozone turbulent fluxes according to *Webb et al.* [1980]. Lag times between the sonic turbulence data and the fast ozone data were determined by regression analysis, and the ozone data were advanced by the determined lag time (typically 6–7 s for TexAQS 2006) to bring the ozone data into synchronization with the wind velocity [see *Bariteau et al.*, 2010].

[13] The turbulent fluxes of the momentum, sensible heat, and water vapor were computed using both the eddy correlation (or covariance) method and inertial dissipation (ID) techniques. The eddy correlation method is the most direct, but it is more sensitive to ship motion and flow distortion than the less direct ID method. Turbulent fluxes and mean variables were computed in 10 min chunks from a nominal 1 h time section and then averaged to 1 h. The 10 min covariance and ID fluxes were selected for quality criteria, and those that passed were averaged in 1 h blocks. ID flux estimates were computed from the variance spectral density of the streamwise wind velocity component, temperature, and humidity in the inertial subrange of locally isotropic turbulence as described by *Fairall et al.* [1997]. The inertial subrange is typically located at frequencies sufficiently above the wave-induced platform motions so corrections are not needed. Direct flux measurements were also accompanied by bulk estimations based on the COARE 3.0 bulk algorithm [*Fairall et al.*, 1996b, 2003].

[14] The fast turbulent flux measurements were accompanied by measurements of standard mean meteorological variables, radiative fluxes, and the atmospheric boundary layer soundings. Mean wind speed magnitude and direction were obtained from the sonic anemometer after transformation to fixed Earth coordinates. A conventional combined temperature/relative humidity (RH) sensor (Väisäla HMP-235 with 0.1°C and 2% RH quoted accuracy) in an aspirated radiation shield was used to determine mean air temperature and humidity. The sea surface temperature was measured with a specially developed floating temperature sensor (called a "sea snake") which sampled at a nominal depth of about

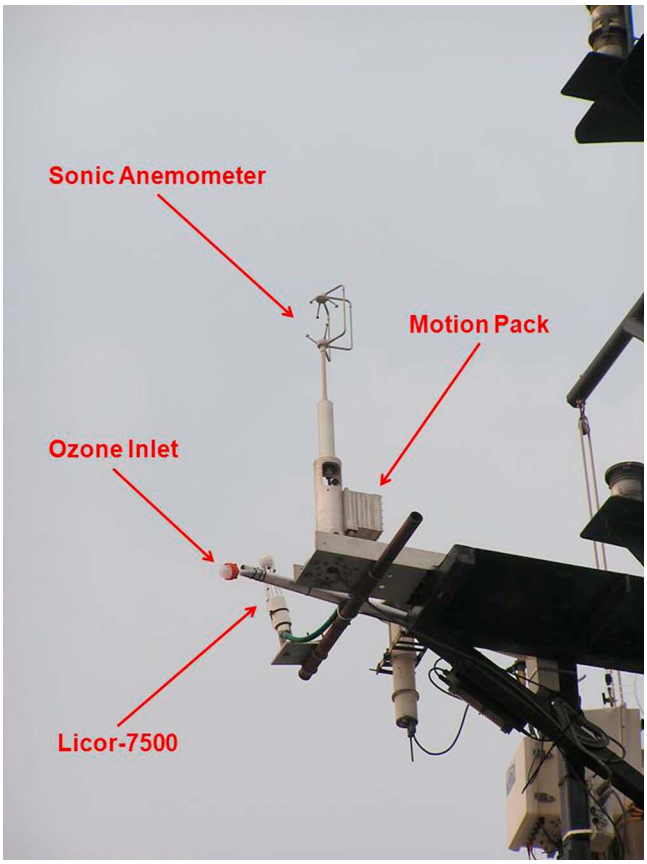

Figure 2. Photo of the deployment arrangement of the ETL/ESRL Turbulent Flux System during the TexAQS 2006 field campaign. Shown here is the forward platform on the jack-staff onto which the sonic anemometer/thermometer Gill/IN USA R3A with the Systron-Donner motion-measurement sensors in the box behind the sonic anemometer, a fast-response CO_2/H_2O Licor-7500 sensor, and ozone inlet with filter (forward oriented pipe) are deployed.

5 cm. This sensor fully resolves the diurnal warm layer, and the interface temperature is obtained by subtracting a cool-skin correction [*Fairall et al.*, 1996a].

[15] In the past two decades, the seagoing flux system has been deployed in a number of field programs in different regions of the world's oceans. The basic ship-based flux measuring system and software have remained essentially the same over this time period, but sensor models, data acquisition system, etc., have been upgraded through the years. As a result of the multiple shipboard deployments of this system, the experience and measurement technique improvements are utilized for investigations of the air-sea fluxes [*Fairall et al.*, 2003]. During the past few years, direct measurements of carbon dioxide fluxes have been added to the suite of instruments (in collaboration with scientists at LDEO and WHOI) [*McGillis et al.*, 2001a, 2001b, 2004]. The series of GasEx cruises focused on carbon dioxide gas flux measurements using the flux system with open-path and closed-path gas analyzers. These integrated systems have been deployed in the midlatitude Atlantic Ocean (GasEx-1998), the Indian and western Pacific Oceans (JASMINE/Nauru99), and the equatorial Pacific Ocean (GasEx-2001). The resulting data sets have been used to make improvements to gas transfer parameterizations [*Fairall et al.*, 2000; *Hare et al.*, 2004] and in investigations to better understand gas transfer physics [*McGillis et al.*, 2004].

3. Turbulent Fluxes and Transfer Coefficients

[16] The turbulent fluxes of momentum (or magnitude of the wind stress), τ, sensible heat, H_S, and latent heat H_L are estimated by the eddy correlation method according to

$$\tau = \tau_x \equiv \rho u_*^2 = -\rho\langle u'w'\rangle, \tag{1}$$

$$H_S = c_p\rho\langle w'T'\rangle, \tag{2}$$

$$H_L = L_e\rho\langle w'q'\rangle, \tag{3}$$

where u_* is the friction velocity, ρ is mean air density, T is the air temperature, q is air specific humidity, c_p is the heat capacity of air at constant pressure, and L_e is the latent heat of evaporation of water. The brackets in equations (1)–(3) denote a time/space average, and u, v, and w are the longitudinal, lateral, and vertical velocity fluctuations about their means. In equation (1), $\tau_x = -\rho\langle u'w'\rangle$ represents the longitudinal (or downstream) component of the wind stress.

[17] The turbulent fluxes, equations (1)–(3), are parameterized by bulk aerodynamic relationships, which relate the fluxes to mean properties of the flow through transfer coefficients, C_D (the drag coefficient), C_H (the Stanton number), and C_E (the Dalton number):

$$\tau = C_D\,\rho U^2, \tag{4}$$

$$H_S = C_H\,\rho\,c_p\,U(T_0 - T_a), \tag{5}$$

$$H_L = C_E\,\rho\,L_e\,U(q_0 - q_a), \tag{6}$$

where U is the mean wind speed at reference height z, and subscripts 0 and a denote their surface and air values, respectively. The specific humidity at sea surface q_0 in equation (6) is 0.98 times the saturation humidity for pure water at the sea surface temperature T_0 to account for the effect of seawater salinity [*Fairall et al.*, 1996b]. Accurate estimation of the transfer coefficients is a crucial problem of air-sea/land interaction. The transfer coefficients depend on stratification and roughness lengths [e.g., *Fairall et al.*, 2003; *Mahrt et al.*, 2003]. The present state-of-the-art parameterization of air-sea surface fluxes is implemented in the COARE 3.0 bulk flux algorithm [*Fairall et al.*, 2003].

[18] Traditionally, the transfer coefficients C_D, C_H, and C_E are adjusted to neutral conditions using Monin-Obukhov similarity theory [*Obukhov*, 1946; *Monin and Obukhov*, 1954]. The neutral counterparts of the drag coefficient, C_{Dn}, Stanton number, C_{Hn}, and Dalton number, C_{En}, are

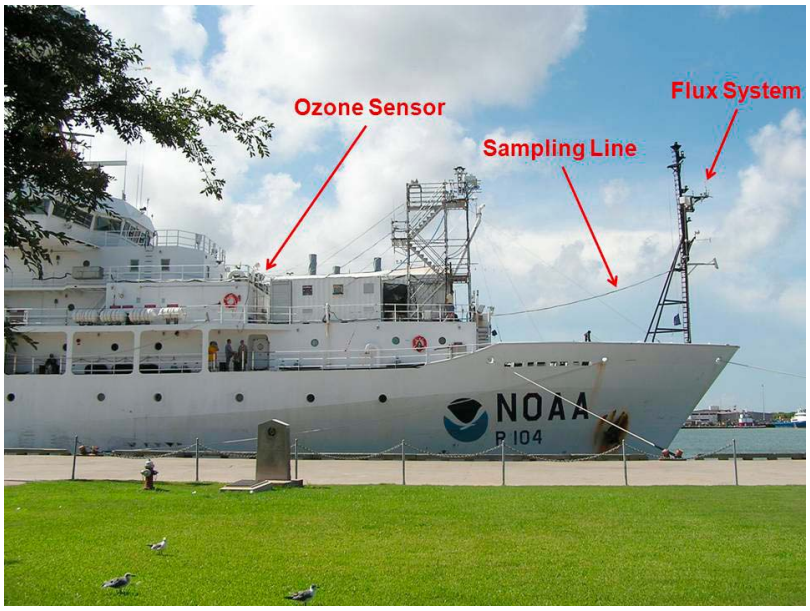

Figure 3. Photo of the NOAA R/V *Ronald H. Brown* in the port of Galveston, Texas, showing the turbulent flux system mounted on the ship foremast (on the right side). The ozone sampling line is running between the foremast and the ship's third deck, where the ozone analytical instrumentation was located.

derived from the following relationships [e.g., *Grachev et al.*, 1998]:

$$C_{Dn}^{-1/2} = C_D^{-1/2} + \frac{\Psi_m}{\kappa}, \tag{7}$$

$$\frac{C_{Dn}^{1/2}}{C_{Hn}} = \frac{C_D^{1/2}}{C_H} + \frac{\Psi_h}{\kappa}, \tag{8}$$

$$\frac{C_{Dn}^{1/2}}{C_{En}} = \frac{C_D^{1/2}}{C_E} + \frac{\Psi_h}{\kappa}. \tag{9}$$

The stability functions, Ψ_m and Ψ_h, must be specified as a function of a stability parameter, $\zeta \equiv z/L$, defined as the ratio of z and the Obukhov length scale, L [*Obukhov*, 1946]:

$$\zeta = \frac{z}{L} = -\frac{z\,\kappa\, g\langle w'\theta_v'\rangle}{u_*^3\,\theta_v}, \tag{10}$$

where θ_v is the virtual potential temperature, κ is the von Kármán constant, and g is the acceleration due to gravity. In this study, we use the formulations of Ψ_m and Ψ_h in equations (7)–(9) from *Fairall et al.* [2003] and the traditional value of $\kappa = 0.4$ for both wind speed and temperature/humidity profiles. Similarity for temperature and humidity profiles is assumed.

[19] The transfer coefficients for neutral conditions (7)–(9) uniquely define the aerodynamic roughness length, z_0, and scalar roughness lengths for temperature, z_{0t}, and humidity, z_{0q} [e.g., *Grachev et al.*, 1998]:

$$z_0 = z\exp\left(-\frac{\kappa}{\sqrt{C_{Dn}}}\right),\quad z_{0t} = z\exp\left(-\frac{\kappa\sqrt{C_{Dn}}}{C_{Hn}}\right),$$
$$z_{0q} = z\exp\left(-\frac{\kappa\sqrt{C_{Dn}}}{C_{En}}\right). \tag{11}$$

Both the transfer coefficients for neutral conditions in equations (7)–(9) and the roughness lengths (11) in this study are expressed relative to the measurement height $z = 18$ m.

4. Measurements Over Different Surfaces

[20] The data collected on board the R/V *Ronald H. Brown* during the TexAQS 2006 campaign permit comparison of turbulent fluxes measured over different footprint surfaces including relatively smooth water surfaces (the Gulf of Mexico and nearby bays and harbor areas) and aerodynamically rough urban/suburban inland areas along ship channels and rivers. For general postcruise analysis, the R/V *Ronald H. Brown* position was classified into one of ten major categories listed below. Details of the classification can be found on the site of the NOAA Pacific Marine Environmental Laboratory (PMEL) Atmospheric Chemistry Group (http://saga.pmel.noaa.gov/Field/TEXAQS/post_cruise_data/; Sara Tucker, personal communication, 2008). The categories (or location codes) from 1 to 10 are: (1) Gulf of Mexico; (2) Galveston Bay (covering ~1500 km^2, 50 km long, 27 km wide, and on average 3 m deep); (3) Port of Galveston (located on the north side of the east end of Galveston Island between the Gulf of Mexico and Galveston Bay); (4) Sabine River and Sabine Lake (vicinity of the city of Port Arthur, Texas); (5) Beaumont, Texas (located on the banks of the Neches River northwest of Sabine Lake, about 48 km upstream from the Gulf of Mexico; with Port Arthur and Orange, it forms a major industrial area on the Gulf Coast); (6) Barbour's Cut Container Terminal (Barbour's Cut is an area of ~546 acres that is located along the Houston Ship Channel and is an industrial port area); (7) Houston Ship Channel between the Turning Basin and east end of the Galveston Bay (except the Barbour's Cut and Jacintoport terminals); (8) Freeport Harbor (Freeport, Texas, is adjacent to the Gulf of Mexico and lies about 80 km southeast of Houston and includes

large chemical plant complex); (9) Matagorda Bay and Alcoa (Matagorda Bay is a large estuary bay on the Texas coast, 910 km^2 in area, separated from the Gulf of Mexico by Matagorda Peninsula; the Alcoa aluminum plant is located at Point Comfort); and (10) Jacintoport Terminal (sitting on 125 acres, Jacintoport is a general cargo terminal located on the north side of the Houston Ship Channel near Channelview, Texas).

[21] The choice of the above categories was motivated by the aim of the program to study industrial emissions which contribute to the air pollution in the Greater Houston Metropolitan Area. For this reason, the ship was positioned in the Houston Ship Channel over a long period of time. The Turning Basin is the navigational head of the channel and is only 12 km from downtown Houston. The proximity to Texas oilfields has led to the establishment of one of the world's greatest concentrations of industrial facilities, including numerous petrochemical refineries and diverse public and private facilities along the channel waterway. These fixtures can be considered as canopies of large-scale roughness elements that characterize this urban area. The height, shape, and distribution density of roughness elements are important factors which affect turbulent exchange between the surface and the atmosphere.

[22] However for our purposes, it is convenient to break up the R/V *Ronald H. Brown* position into three sampling categories: (1) open sea locations; (2) bays, lakes, and near coastal harbor areas; and (3) urban/suburban inland locations. The first category includes the Gulf of Mexico (location code 1); the second category includes the Galveston Bay (location code 2), Sabine River and Sabine Lake (location code 4), Freeport Harbor (location code 8), and the Matagorda Bay (location code 9); the third category includes Port of Galveston (location code 3), City of Beaumont (location code 5), Barbour's Cut (location code 6), Houston Ship Channel (location code 7), and Jacintoport (location code 10).

[23] Figure 4 shows plots of the bin-averaged and individual 1 h data of the measured turbulent fluxes, equations (1)–(3), at the reference height z versus their bulk counterparts, equations (4)–(6), for the data collected over coastal waters of the Gulf of Mexico. The turbulent fluxes are based on both covariance and inertial dissipation (ID) estimates. The COARE algorithm for open ocean conditions [*Fairall et al.*, 2003] was used to compute bulk fluxes. The individual 1 h averaged data are also shown in Figure 4 as open pink circles and open green triangles. These points give an estimate of the available data and the typical scatter of the data. It should be noted that all bulk algorithms (as well as ID technique) predict only the downstream component of the wind stress (τ_x) because the standard Monin-Obukhov similarity theory is based on the assumption that stress and wind vectors are aligned in the same direction; that is, the lateral (or crosswind) stress component $\tau_y = -\rho\langle v'w'\rangle = 0$ by definition. For this reason, eddy covariance stress, C_D, C_{Dn}, and $\zeta \equiv z/L$ in Figure 4 and other plots are based on the definition (1). Our analysis in Figure 4 suggests very close agreement between the air-sea fluxes (especially for τ_x; see Figure 4a) measured over coastal waters of the Gulf of Mexico during TexAQS 2006 and the model estimations. Deviations of τ_x covariance values from the bulk estimates in Figure 4a are associated with light winds (less than about 4 m s^{-1}). Note that direct flux measurement at low winds is a perplexing issue. According to Figures 4b and 4c the bulk algorithm overestimates the sensible and latent heat flux by ~10%. This discrepancy may be associated with possible coastal influences on the sensible and latent heat fluxes. Note also that a number of the individual 1 h points in Figure 4b are not statistically representative for $H_S > 15$ W m^{-2}. It should be mentioned that the data collected during the TexAQS 2006 field campaign show that air-sea fluxes measured over the Gulf of Mexico are less affected by coastal effects as compared to the fluxes measured over the Gulf of Maine during the New England Air Quality Study (NEAQS) 2004 field campaign [*Fairall et al.*, 2006]. This may suggest that coastal effects have less influence on air–sea interaction in a coastal zone for convective conditions observed during TexAQS 2006 both over sea and land (see time series for $\zeta \equiv z/L$ in section 5). During the NEAQS 2004 field campaign conducted in July and August 2004, shallow stable boundary layers over the cool waters of the Gulf of Maine (between Cape Cod and Nova Scotia) have been reported [*Angevine et al.*, 2006; *Fairall et al.*, 2006].

[24] A similar analysis in terms of true wind direction is shown in Figure 5. According to Figure 5, both covariance and ID estimates of the scalar heat fluxes H_S (Figure 5b) and H_L (Figure 5c) normalized by the appropriate bulk values are not correlated with wind direction within the accuracy of the experimental data. The scatter of latent heat flux observations is lower as compared to the sensible heat flux because over the ocean H_L is generally an order of magnitude larger than H_S, and therefore the ratio of H_L to its bulk value is less noisy. However, both normalized scalar fluxes H_S and H_L are less sensitive to the wind direction than the momentum flux. Although the ratio of measured momentum flux (downstream component of the wind stress) to the appropriate bulk flux (4) for ID estimates is not correlated with wind direction, the uw covariance of the momentum flux is more sensitive to the wind direction and the data have greater scatter (Figure 5a). Bin-averaged medians of the normalized covariance estimates in Figure 5a substantially exceed unity for two wind sectors, for winds from about 60° to 120° and from 250° to 320° (offshore flow). Both these cases are associated with light winds (not shown) and are correlated with deviations of the uw covariance from the bulk estimates in Figure 4a. Note that coastal influence and ocean surface wave effects on the momentum flux at low winds are possible explanations for the reported deviations.

[25] Figures 6 and 7 show similar analyses for data collected over the bays, lakes, and near coastal harbor areas (location codes = 2, 4, 8, and 9), but the number of usable observations in this case is lower and less convincing than for measurements over the Gulf of Mexico in Figures 4 and 5. Figure 6 shows that, as a first approximation, the bulk algorithm [*Fairall et al.*, 2003] still can be used to describe the turbulent fluxes (except the uw covariance at light winds; see Figure 6a) in this case. The agreement with the COARE algorithm is within the accuracy of the experimental data. We have found that most of the averaged experimental points lie within one standard deviation in terms of the error bars. The data presented in Figure 7 provides additional support confirming that the normalized scalar fluxes H_S and H_L are less sensitive to wind direction than the momentum flux (cf. Figure 5). Note the different scales in the vertical axes for the momentum and scalar fluxes in Figure 7.

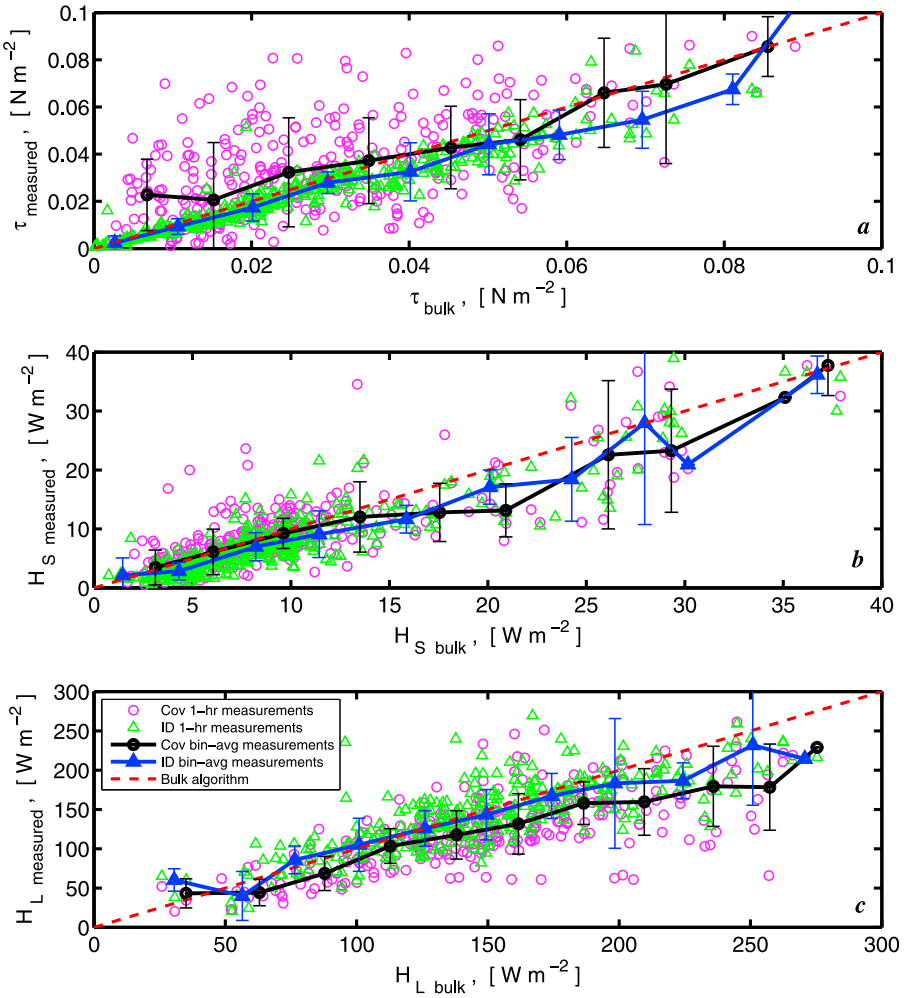

Figure 4. Bin-averaged medians (solid lines) and individual 1 h data (open pink circles and open green triangles) of the measured turbulent fluxes (equations (1)–(3)), of (a) momentum (downstream component of the wind stress), (b) sensible heat, and (c) latent heat versus their bulk counterparts (equations (4)–(6)) for the data collected over coastal waters of the Gulf of Mexico (location code 1). The turbulent fluxes are based on both covariance estimates (solid black circles) and inertial dissipation (ID) technique (solid blue triangles). The COARE algorithm [*Fairall et al.*, 2003] was used to compute the bulk fluxes (dashed lines). Error bars show the standard deviation of the binned data points. Width of bins is 0.01 Nm^{-2} (Figure 4a), 4 Wm^{-2} (Figure 4b), and 25 Wm^{-2} (Figure 4c).

[26] As might be expected, the observed turbulent exchange inland differs widely from the bulk model predictions. According to Figure 8a, C_{Dn} based on the *uw* covariance increases dramatically over urban areas (location codes: 3, 5–7, and 10), and the average value can be an order of magnitude larger than over the sea surface that corresponds to an aerodynamic roughness length (11), $z_0 \approx$ 0.5–1 m (not shown). These results are in reasonable agreement with previously reported values of C_{Dn} and z_0 over urban areas [e.g., *Grimmond et al.*, 1998, Figure 3; *Grimmond and Oke*, 1999, Table 6; *Roth*, 2000, Table A.1; *Klipp*, 2007, Figure 2]. This sharp change in the momentum flux and the drag coefficient for sea-land transition is clearly due to the change in aerodynamic properties of the surface. An elevated value of C_{Dn} can be due to an elevated u_*, reduced U, or both. It is agreed that increasing u_* over rough urban surfaces is caused by contributions from the form drag owing to pressure differentials between the windward and leeward sides of buildings and other structures [e.g., *Raupach*, 1992; *Shao and Yang*, 2005]. According to the model of *Coceal and Belcher* [2004], urban canopy stress acts to decelerate the wind speed within the canopy. Both of these effects can contribute significantly to the drag coefficient over a rough urban surface. For example, individual 1 h averaged values of C_{Dn} can be two orders of magnitude larger than over-sea surface values (see the time series in section 5).

[27] According to Figures 8b and 8c, such a strong relative increase is not observed for the sensible and latent heat transfer. In contrast to C_{Dn}, the neutral Stanton and Dalton numbers measured over land are not significantly different from the over-sea measurements (dashed lines in Figure 8). However, even the observed increase in C_{Hn} and C_{En} for inland conditions may be associated with the procedure of using the surface temperature measurement from R/V *Ronald H. Brown* (see the time series in section 5). The surface

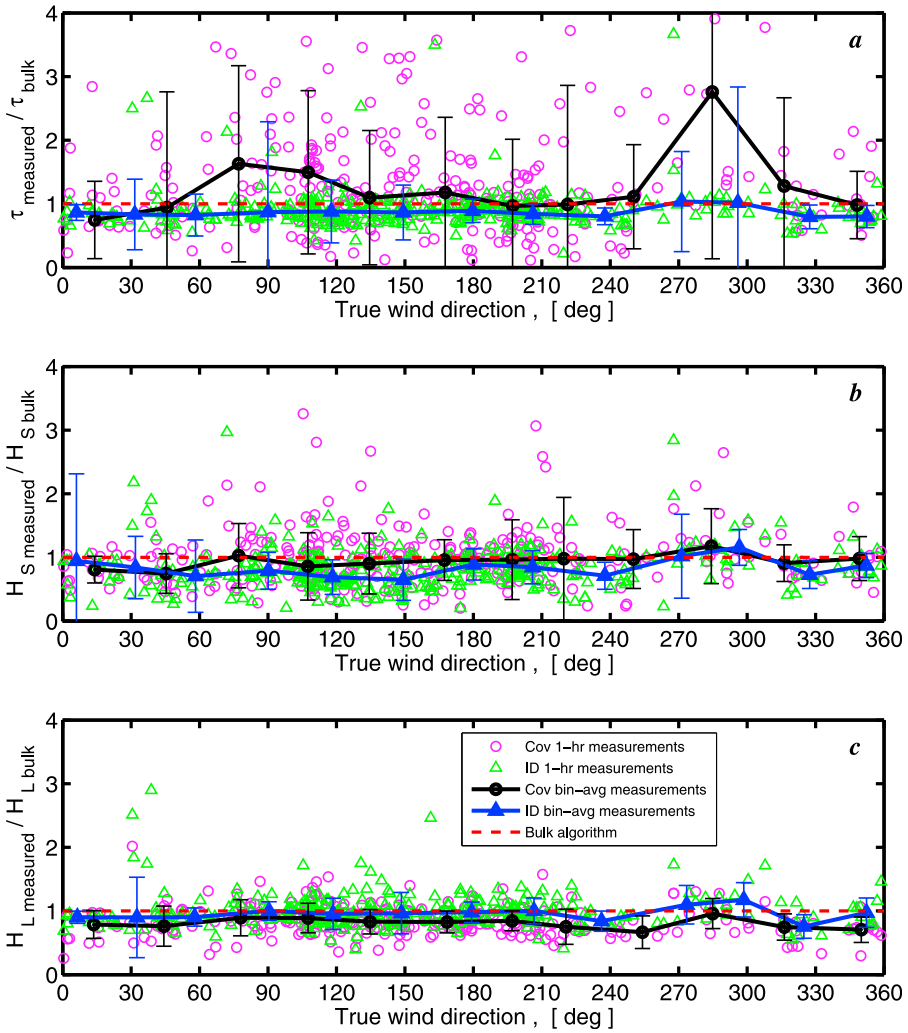

Figure 5. Bin-averaged medians (solid lines) and individual 1 h data (open pink circles and open green triangles) of the ratios of measured turbulent fluxes (equations (1)–(3)) to the appropriate bulk estimates (equations (4)–(6)) for (a) momentum (downstream component of the wind stress), (b) sensible heat, and (c) latent heat fluxes versus true wind direction for the data collected over coastal waters of the Gulf of Mexico (location code 1). The turbulent fluxes are based on both covariance estimates (solid black circles) and inertial dissipation (ID) technique (solid blue triangles). The COARE algorithm [*Fairall et al.*, 2003] was used to compute the bulk fluxes (dashed lines). Error bars show the standard deviation of the binned data points. Width of bins is 30°.

temperature in equations (5) and (6) is water temperature in a ship channel measured by a floating "sea snake" thermometer at ~5 cm depth. This water surface temperature is thought to be generally lower than the surface temperature of the surrounding land at midday which is appropriately associated with C_{Hn} and C_{En}. To avoid this problem, data for C_{Hn} and C_{En} presented in Figures 8b and 8c are restricted to night conditions when the measured water temperature should be close to the land footprint temperature. For this reason the number of points in Figures 8a and 8b is less than in Figure 8a plotted for both day and night conditions. This issue is also discussed further in section 5.

[28] According to Figures 4 and 5, both the direct covariance and ID turbulent flux estimates are in close agreement for measurements over the Gulf of Mexico (location code 1). According to Figure 8, there is a discrepancy between these two methods for overland measurements for light winds that are probably indicative of the low-frequency contribution in the covariance flux estimates for these cases.

[29] For overland situations, the measurement height (18 m) was usually above the canopies of typical roughness elements (e.g., trees, cargo containers, parking lots with cars, low commercial-industrial buildings, etc.) along the ship channel. However, the turbulent measurements made aboard the R/V *Ronald H. Brown* along the Houston Ship Channel during the TexAQS 2006 field campaign should be classified as measurements within the urban roughness sublayer, where individual roughness elements result in a flow and turbulence field that can be horizontally and vertically inhomogeneous [e.g., *Raupach et al.*, 1991; *Rotach*, 1993, 1999; *Kastner-Klein and Rotach*, 2004; *Christen et al.*, 2009, and references therein]. It has indeed been

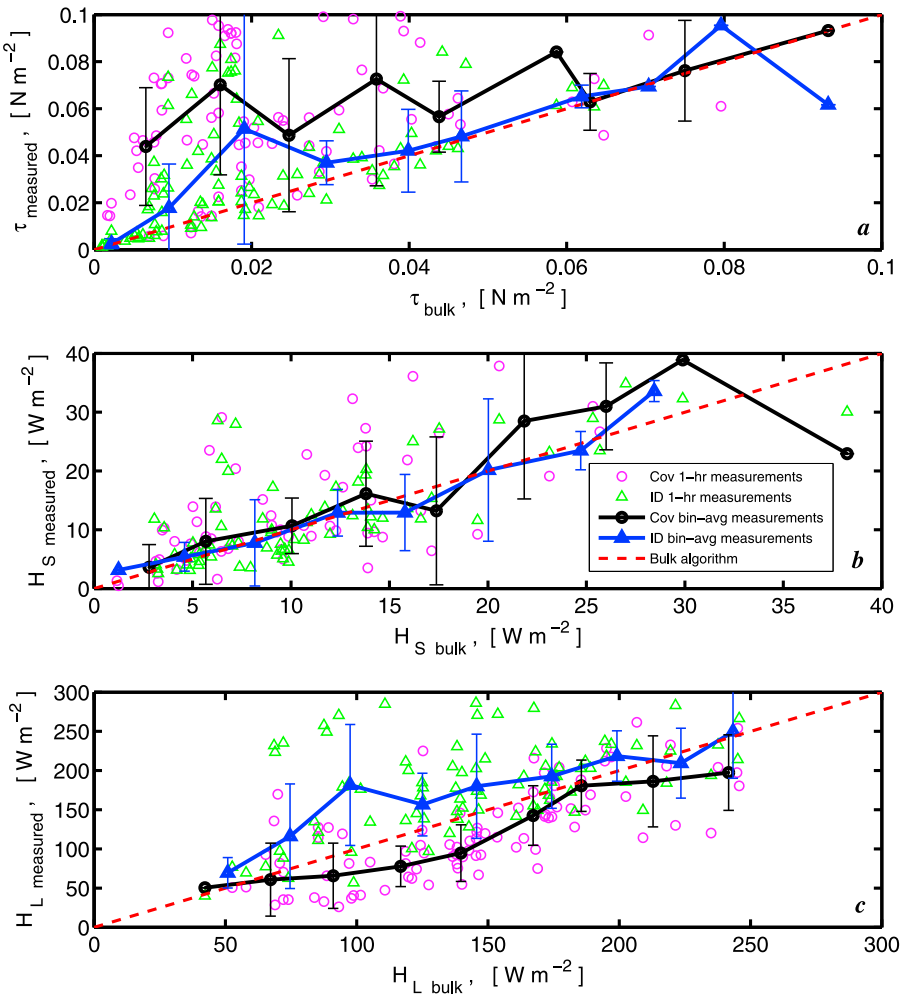

Figure 6. Same as Figure 4 but for data collected over the bays, lakes, and near coastal harbor areas (location codes 2, 4, 8, and 9). Notation is the same as in Figure 4.

demonstrated, that the roughness sublayer for built-up areas extends from the surface to roughly 2–5 times the height of typical roughness elements [e.g., *Raupach et al.*, 1991]. Nevertheless, turbulent measurements are more interesting inside the urban roughness sublayer where most people live and the majority of pollutants are emitted. Although field measurements in the urban roughness sublayer pose a challenge for traditional methods and the obtained results must be interpreted carefully because the theoretical assumptions (e.g., horizontal homogeneity of the flow field) cannot be fulfilled, there are no principal limitations for eddy covariance fluxes. Because most human activities in cities take place within the urban roughness sublayer, turbulent measurements from TexAQS 2006 along the Houston Ship Channel can provide valuable information on statistics needed for dispersion modeling or energy and mass exchange in the Houston metropolitan area.

5. Time Series

[30] Although plots of the bin-averaged turbulent fluxes and the transfer coefficients in Figures 4–8 are useful for averaged analyses, additional detailed information can be obtained from the time series of these and other relevant variables plotted for over-sea and overland conditions. Figures 9–11 show typical time series of hourly averages of the location codes, the basic meteorological variables, turbulent fluxes, and transfer coefficients collected during the cruise leg 1 (4–16 August 2006; YD 216–228). Similar typical time series for leg 2 including the duration of stay at the Port of Galveston (18–30 August 2006; YD 230–242) are shown in Figures 12–14.

[31] The time series of solar radiation in Figures 9d and 12d provide a reference to local day and nighttime. According to Figures 11d and 14d, for the most part, the atmospheric boundary layer observed in TexAQS 2006 both over sea and land during day and night was unstable ($z/L < 0$, see equation (10)). Measurements made inland show the strong diurnal cycle of the basic meteorological variables and fluxes, but diurnal variations are suppressed when the ship was in the Gulf of Mexico (see Figures 9 and 12 for different location codes).

[32] The time series in Figures 11a and 14a clearly demonstrate a sharp change of C_{Dn} for transitions from sea to land and back. This is especially revealed as a step-like behavior of C_{Dn} in Figure 14a when the ship was in the Port of Galveston during 4 days (YD ≈ 230.5–234.5 UTC, location code 3; see Figure 12a) and in Barbour's Cut

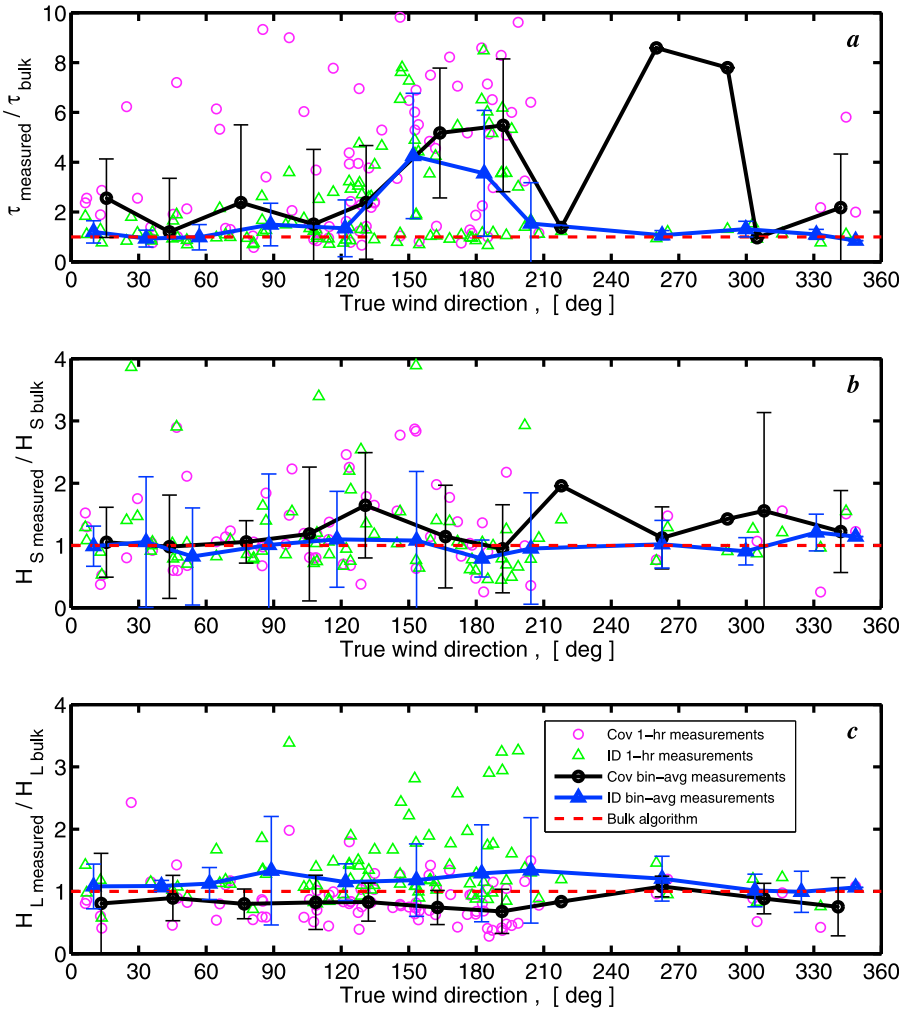

Figure 7. Same as Figure 5 but for data collected over the bays, lakes, and near coastal harbor areas (location codes 2, 4, 8, and 9). Notation is the same as in Figure 5. Note different scales in the vertical axes for the momentum and scalar fluxes.

Terminal of the Port of Houston during 2 days (YD ≈ 238–240 UTC, location code 6; see Figure 12a). It is particularly remarkable that the magnitude of the neutral drag coefficient in these two episodes (YD ≈ 230.5–234.5 and 238–240 UTC) remains approximately constant while the wind speed (Figure 12c) and the wind stress (Figure 13a) show diurnal variations. According to Figures 11a and 14a, individual 1 h points can reach $C_{Dn} \approx 0.1$ value that is approximately two orders of magnitude larger than typical over-sea surface values.

[33] However, similar step-like behavior was not observed for C_{Hn} (Figures 11b and 14b) and C_{En} (Figures 11c and 14c). The neutral Dalton number does not change significantly for transitions from sea to land and back. Figures 11b and 14b show an increase of C_{Hn} inland, but this effect has a diurnal cycle, in contrast to the drag coefficient, and it is associated with the traditional diurnal cycle of the sensible heat flux over land (Figures 10b and 13b) and with the underestimation of the surface temperature as mentioned in section 4. The diurnal variations of the incoming short-wave solar radiation (Figures 9d and 12d) over land cause diurnal variations of the land surface temperature and therefore the sensible heat flux. However, the ship observes the local water temperature in channels or rivers, and during daytime periods, this temperature is certain to be sufficiently less than the spatially averaged land temperature. One may suggest that C_{Hn} will not change significantly over different surfaces (similar to C_{En}) if proper overland surface temperature with the diurnal cycle is used in equation (5). One may also expect that during a night, the water temperature measured in the ship channel will be closer to averaged land surface temperature. Figures 8b and 8c plotted for night conditions and minimum values of C_{Hn} (i.e., during nights) in Figures 11b and 14b in some sense support this suggestion. To a lesser degree, the underestimation of the surface temperature may also affect the Dalton number analysis. Note also, that the Dalton number in (6) is based on the assumption that the near-surface specific humidity is 98% of the saturation specific humidity at the observed surface temperature, and this assumption is not valid over land.

[34] Although water surface temperature is substantially lower than the surface temperature of the surrounding land

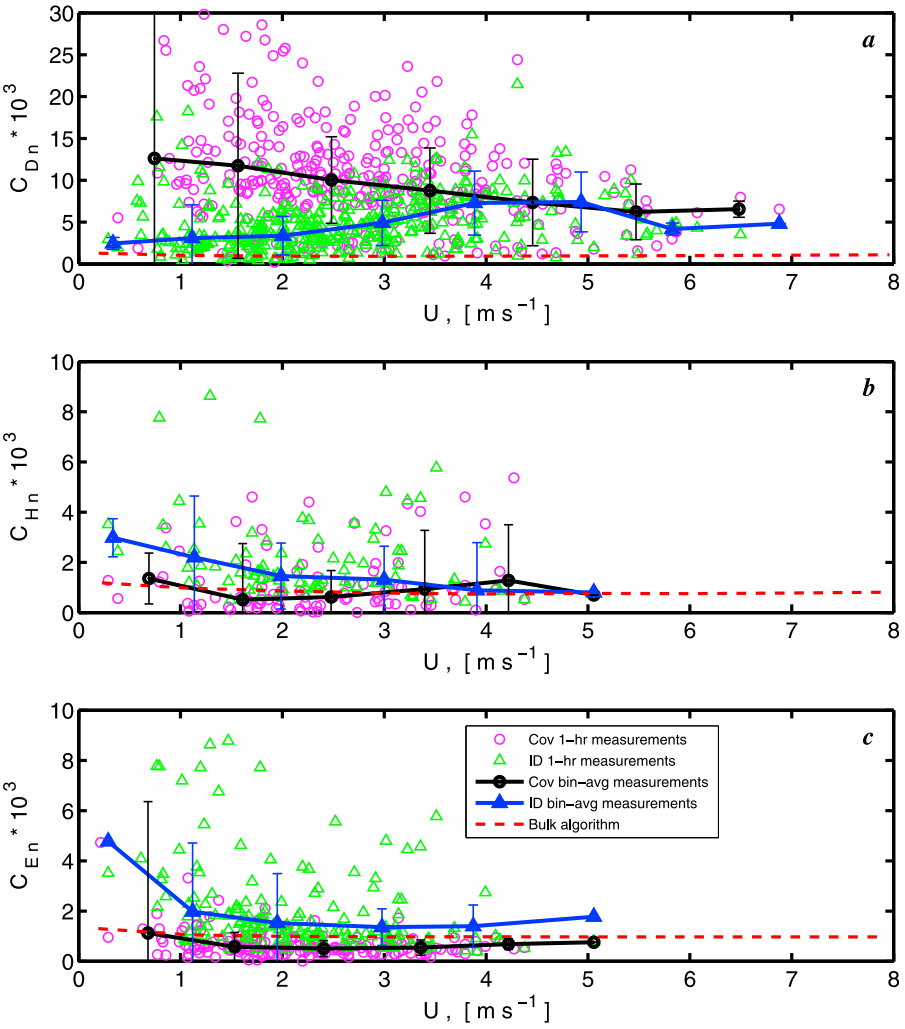

Figure 8. Bin-averaged medians (solid lines) and individual 1 h data (open pink circles and open green triangles) of (a) neutral drag coefficient (equation (7)), (b) Stanton number (equation (8)), and (c) Dalton number (equation (9)) versus mean wind speed for the data collected over land (location codes 3, 5–7, and 10). Data presented in Figures 8b and 8c were collected only during night. The turbulent fluxes are based on both covariance estimates (solid black circles) and inertial dissipation (ID) technique (solid blue triangles). The COARE algorithm [*Fairall et al.*, 2003] was used to compute bulk transfer coefficients (dashed lines) for comparison. Error bars show the standard deviation of the binned data points. Width of bins is 1 m s^{-1}.

surfaces at midday it is generally higher at midnight due in part to a rather high thermal inertia of water. Temperature of the surrounding land surfaces can change considerably during the diurnal cycle and usually drops at night primarily by radiative cooling accompanied by some convection and conduction. The maximum and minimum temperatures at the land surfaces depend mostly on the extent of buildup of the heat reservoir and its storage capacity. For example, during night temperature of standing water is generally higher than temperature of typical bare soils and rocks but slightly lower than temperature of vegetation (e.g., grass lawns) [*Sabins*, 1987]. In the morning and evening hours temperatures of water and land are approximately equal because of diurnal cycle of the land temperature. Taking into account these thermal crossover points and mixed nature of the land surface (soil, grass, etc.) one may expect that water temperature in channels or rivers more or less correct represents the spatially averaged nocturnal land temperature associated with the observed sensible heat flux.

[35] It is believed that this asymmetric behavior between C_{Dn} and C_{Hn}, C_{En} over urban surfaces is associated with the effect of pressure drag (form drag) induced by the local structures. The urban roughness elements influence the wind profile, and they are presumed to enhance the momentum transfer through pressure terms in the Navier-Stokes equations, whereas the pressure transport does not directly affect the sensible and latent heat flux.

6. Carbon Dioxide and Ozone Turbulent Fluxes

[36] As mentioned in section 2, measurements of carbon dioxide and ozone turbulent fluxes can be made on the basis of the well-established direct covariance (also known as eddy correlation) technique. This method assumes that from

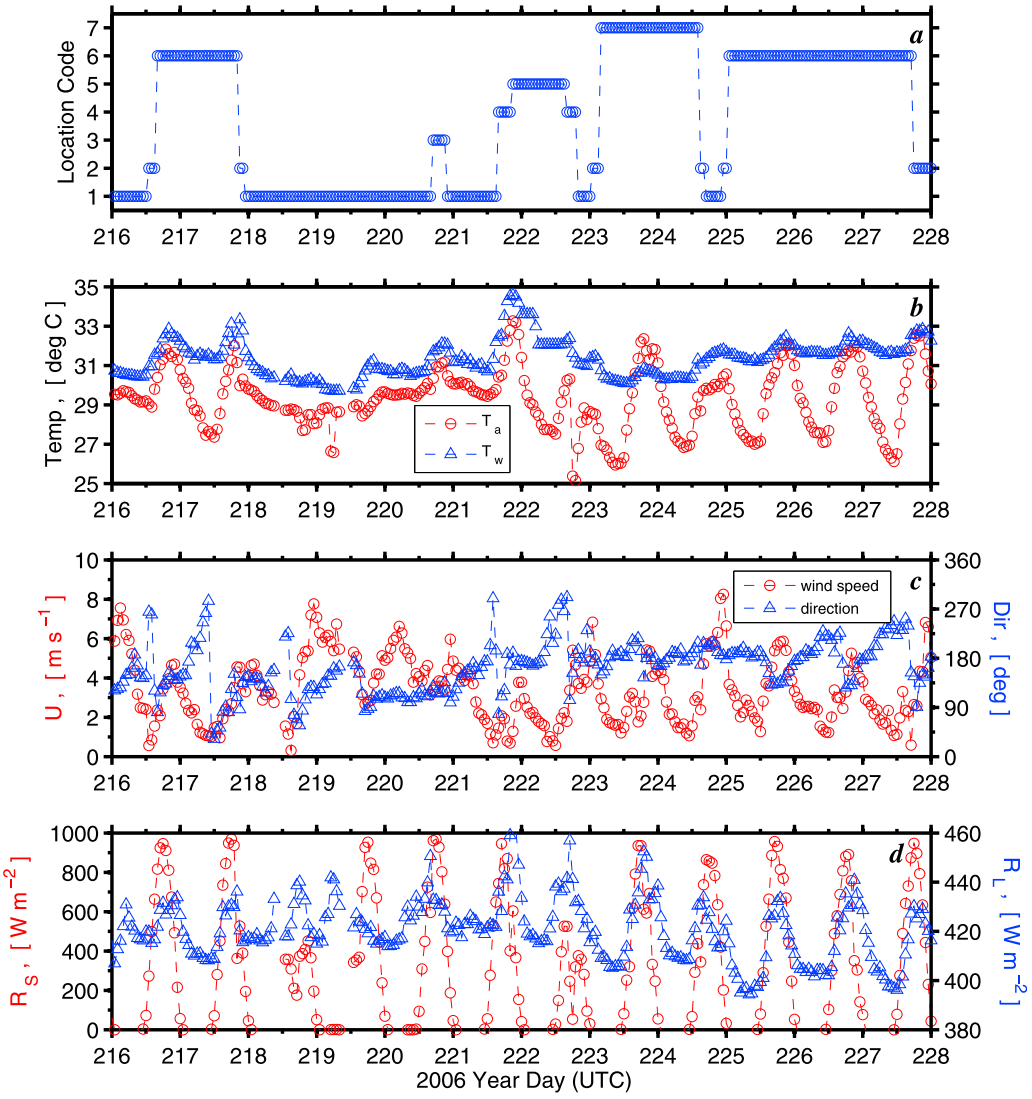

Figure 9. Time series of (a) location code, (b) air and water temperature, (c) wind speed and true wind direction, and (d) short-wave (circles) and long-wave (triangles) radiation for year days 216–228 (4–16 August 2006). The data are based on 1 h averaging.

the Reynolds' decomposition, the turbulent flux F_c of a minor gas can be written as

$$F_c = \langle w\rho_c \rangle = \langle w'\rho_c' \rangle + \langle w \rangle \langle \rho_c \rangle, \tag{12}$$

where ρ_c is the density of a gas. The last term in equation (12) is usually neglected because the mean vertical velocity $\langle w \rangle$ is negligible. However, this term (called WPL or Webb effect after *Webb et al.* [1980]) must be taken into account when the turbulent fluxes of minor constituents such as carbon dioxide, ozone, or, in some cases, water vapor are measured [see also *Webb*, 1982; *Leuning and Legg*, 1982; *Leuning*, 2007]. *Webb et al.* [1980] also showed that the turbulent flux can be expressed in pure eddy covariance form [*Webb et al.*, 1980, equation (20)]

$$F_c = \langle \rho_a \rangle \langle w' r_c' \rangle, \tag{13}$$

when the mixing ratio r_c relative to dry air component is used; that is, $r_c = \rho_c/\rho_a$ (ρ_a is the density of the dry air component). However, if the constituent's specific mass content relative to the total air content, $c = \rho_c/\rho$, is measured, then the Webb correction term to the covariance form $\langle w'c' \rangle$ is required.

[37] In the case of water vapor, this correction is only a few percent over the sea surface, and for this reason the Webb correction term is often omitted in equation (3). However, the correction can well exceed 10% for overland measurements when the Bowen ration, $Bo = H_S/H_L$, is around two or greater [*Webb et al.*, 1980]. As mentioned earlier, the Webb correction was applied to the water vapor, CO_2, and O_3 fluxes in this study.

[38] The direct measurements of the ozone turbulent fluxes near the surface can be also used to characterize the deposition velocity, V_d. In atmospheric chemistry, the deposition velocity is defined as the ratio of the flux of a substance, F_c, to its concentration in the atmosphere $c = \rho_c/\rho$:

$$V_d = -\frac{F_c}{c}. \tag{14}$$

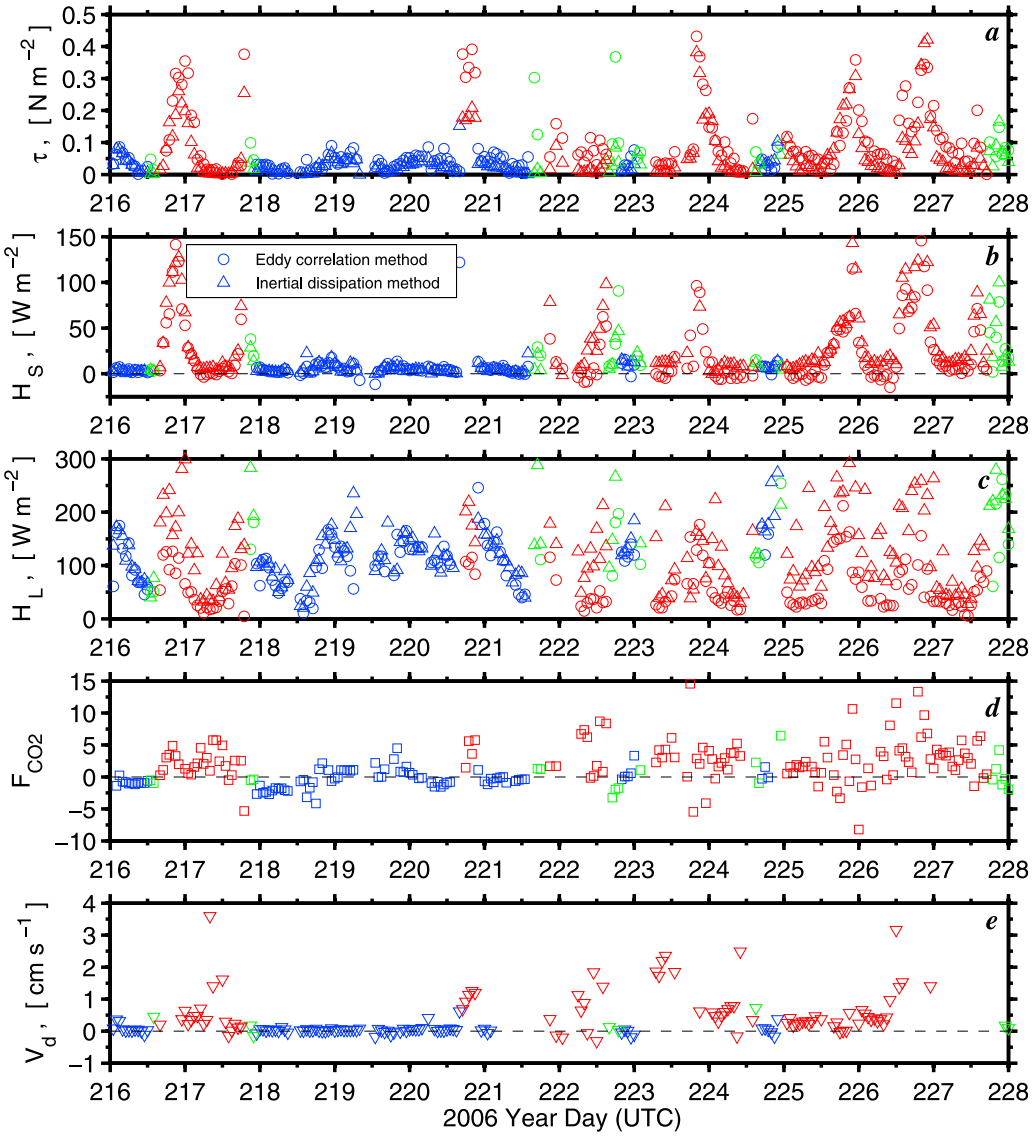

Figure 10. Time series of (a) wind stress, (b) sensible heat flux, (c) latent heat flux, (d) CO_2 turbulent flux (eddy covariance), and (e) ozone deposition velocity (equation (14)) for year days 216–228 (4–16 August 2006). The data are based on 1 h averages of 10 min flux estimates. The turbulent fluxes τ, H_S, and H_L in Figures 10a–10c are based on both covariance (circles) and the ID (triangles) estimates. Blue corresponds to the data collected over coastal waters of the Gulf of Mexico (location code 1); green corresponds to the data collected over the bays, lakes, and near coastal harbor areas (location codes 2, 4, 8, and 9); and red corresponds to the data collected over land (location codes 3, 5–7, and 10). The unit of measurement of CO_2 flux (Figure 10d) is μmol m s^{-1}.

The deposition velocity (14) is defined as positive for a surface sink and vice versa (i.e., a negative deposition velocity implies a surface source). In the case of negative deposition velocity, V_d in equation (14) can be viewed as an "exchange" velocity. The deposition velocity (14) is a traditional parameter for atmospheric ozone transfer studies [e.g., *Fairall et al.*, 2006]. On the other hand, in CO_2 flux studies, it is common to use transfer velocities to characterize the sublayer transfers [e.g., *Fairall et al.*, 2000; *McGillis et al.*, 2001a, 2001b, 2004; *Hare et al.*, 2004]. The gas transfer velocity is defined similar to equation (14), but instead of the concentration in the denominator of equation (14), the surface-air concentration difference is used. Because concentration of carbon dioxide at the surface in this cruise has not been evaluated, the gas transfer velocity is not computed here.

[39] The time series in Figures 10d, 10e, 13d, and 13e show that both CO_2 and O_3 turbulent fluxes measured over land were larger in magnitude and have higher variability compared to the over water measurements (see also ozone data analysis by *Bariteau et al.* [2010]). Figure 15 shows carbon dioxide and ozone turbulent fluxes, and the ozone deposition velocity (14) versus the wind speed measured for three sampling categories defined earlier (the Gulf of Mexico, harbors/bays, and inland), Table 1 lists averaged values (medians) of the CO_2 and O_3 turbulent fluxes and the O_3 deposition velocity for each location code. According to our

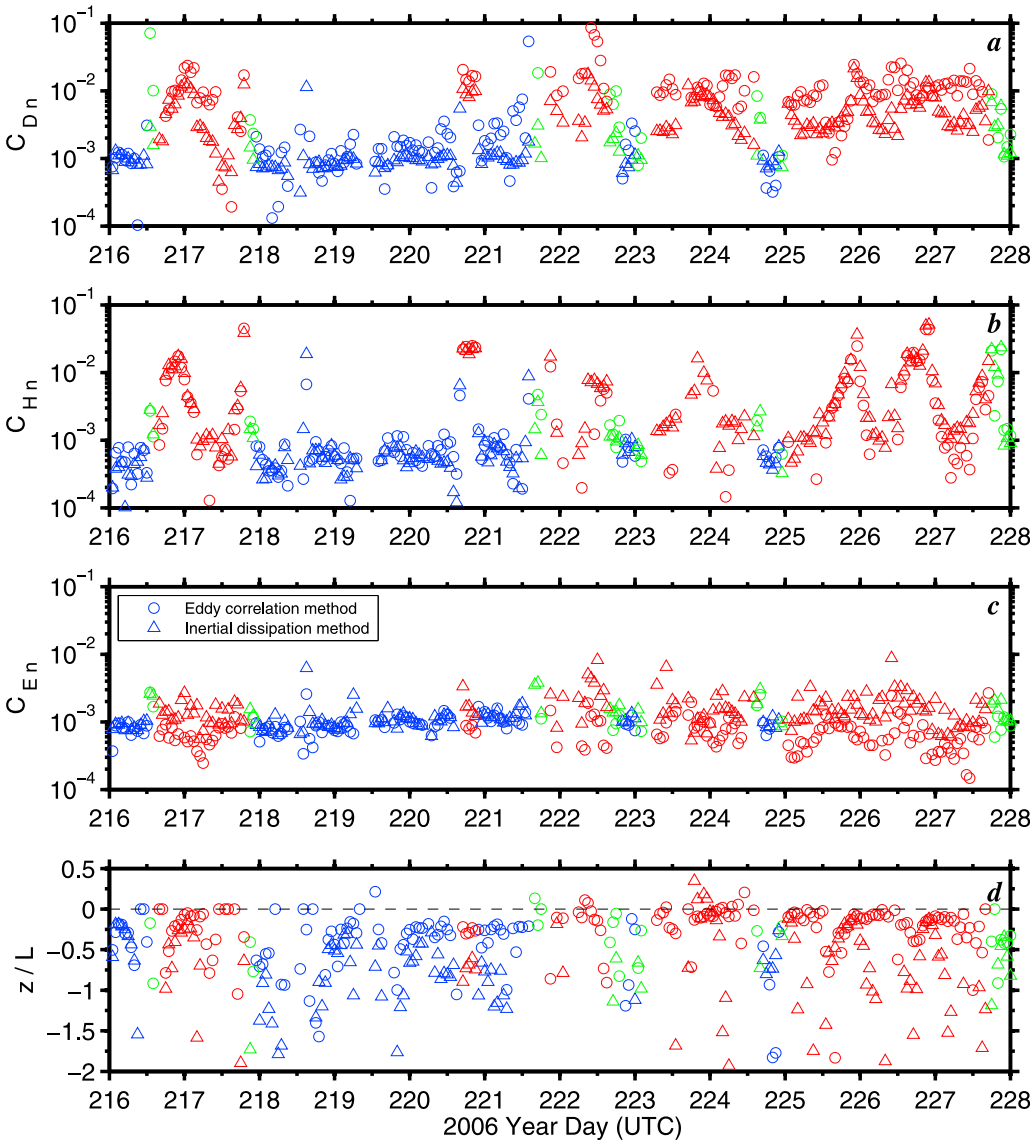

Figure 11. Time series of (a) neutral drag coefficient, (b) neutral Stanton number, (c) neutral Dalton number, and (d) Monin-Obukhov stability parameter (equation (10)) for year days 216–228 (4–16 August 2006). The data are based on 1 h averages of 10 min flux estimates. The values of C_{Dn}, C_{Hn}, C_{En}, and $\zeta = z/L$ are based on both covariance (circles) and ID (triangles) estimates. Blue corresponds to the data collected over coastal waters of the Gulf of Mexico (location code 1); green corresponds to the data collected over the bays, lakes, and near coastal harbor areas (location codes 2, 4, 8, and 9); and red corresponds to the data collected over land (location codes 3, 5–7, and 10).

study, the turbulent transfer over different harbors/bays areas (location codes 2, 4, 8 and 9) is mainly an intermediate case between over-sea and overland situations (see Figure 15 and Table 1).

[40] According to Figure 15a, the turbulent flux of carbon dioxide was mostly negative (uptake by the surface) over the waters of the Gulf of Mexico and for some bays (see Table 1), but it becomes positive (release to the atmosphere) when measurements were made inland. Figure 15a shows a weak dependence of the measured fluxes of on the wind speed. The Gulf of Mexico was generally a sink for CO_2 and the median averaged value of the CO_2 turbulent flux was -0.237 μmol m^{-2} s^{-1} ≈ -7.47 mol m^{-2} yr^{-1} (see Table 1) which is consistent (both in the sign and the magnitude) with the results obtained during GasEx-1998 field campaign in the North Atlantic in a warm-core eddy near 46°N and 21°W [*Hare et al.*, 2004, Figures 2 and 6]. Our CO_2 flux data collected over land in the Houston metropolitan area (see Table 1 and Figures 10d, 13d, and 15) are in agreement with other urban studies [e.g., *Grimmond et al.*, 2002, 2004; *Moriwaki and Kanda*, 2004; *Velasco et al.*, 2005, 2009; *Vogt et al.*, 2006], which have shown that an urban/suburban surface is generally a net source of carbon dioxide. The main source of CO_2 is the consumption of fossil fuels, from both vehicles and home heating. The daytime uptake by urban vegetation during a summer day is not strong enough to offset the emissions from anthropogenic sources. Peak values of CO_2 fluxes are generally associated with rush hour traffic.

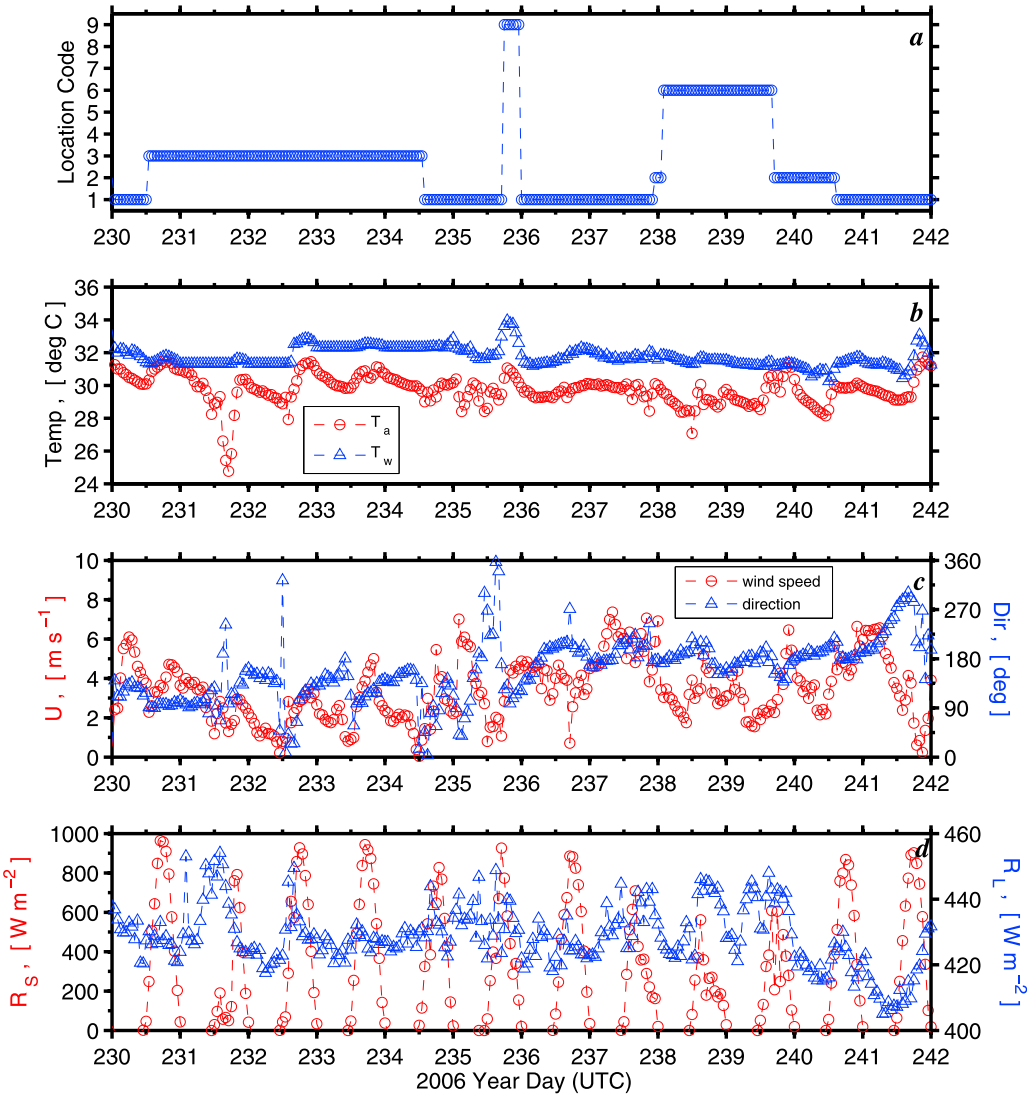

Figure 12. Same as Figure 9 but for data obtained during year days 230–242 (18–30 August 2006).

[41] The averaged CO_2 fluxes in a suburban area of Chicago reported by *Grimmond et al.* [2002, Figure 3b] were always positive in the range 0 to 10 μmol m^{-2} s^{-1}. *Moriwaki and Kanda* [2004] reported CO_2 fluxes measured in a low-storied residential area of Tokyo (Japan). In their study, the flux values range from 0.2 to 0.5 mg m^{-2} s^{-1} ($\approx$ 4.54–11.3 μmol m^{-2} s^{-1}) in July and from 0.2 to 1.1 mg m^{-2} s^{-1} ($\approx$ 4.54–24.9 μmol m^{-2} s^{-1}) in December. During the summer CO_2 emissions tend to be lower, owing to reduced fuel consumption for heating and because trees are in full leaf, increasing the CO_2 uptake by photosynthesis. The CO_2 flux measurements made in a densely populated section of Mexico City during 2003 [*Velasco et al.*, 2005] showed a clear diurnal cycle, and the mean daily CO_2 flux was 0.41mg m^{-2} s^{-1} $\approx$ 9.3 μmol m^{-2} s^{-1}. According to *Velasco et al.* [2009], the fluxes of CO_2 measured in a different district of Mexico City 3 years later were 1.4 times higher than in 2003, mainly because traffic levels were higher near the 2006 site compared to the 2003 site reported by *Velasco et al.* [2005]. In the framework of the Basel Urban Boundary Layer Experiment (BUBBLE, 2001–2002), the CO_2 flux was measured above a street canyon at different heights [*Vogt et al.*, 2006]. According to the BUBBLE campaign, low values of the CO_2 flux of about 3 μmol m^{-2} s^{-1} were measured during the second half of the night. During the daytime, average values reached up to 14 μmol m^{-2} s^{-1}, with peak values of 30 μmol m^{-2} s^{-1}. The magnitude of the average CO_2 flux and the diurnal pattern measured above the densely built-up center of Marseille (France) by *Grimmond et al.* [2004, Figure 10] are comparable to those reported from Basel [*Vogt et al.*, 2006], but these are approximately twice the magnitude of the average values reported in a more residential area of Chicago [*Grimmond et al.*, 2002].

[42] According to our data collected inland, the CO_2 flux was directed upward; that is, the Houston metropolitan area is a net source of CO_2. The average CO_2 flux value measured along the Houston Ship Channel was about 2.8 μmol m^{-2} s^{-1} (Table 1), and daytime 1 h peak values measured inland reached up to 15 μmol m^{-2} s^{-1} (Figure 10d). Our CO_2 fluxes measured inland over a suburban area of Houston roughly equals that reported by *Grimmond et al.*

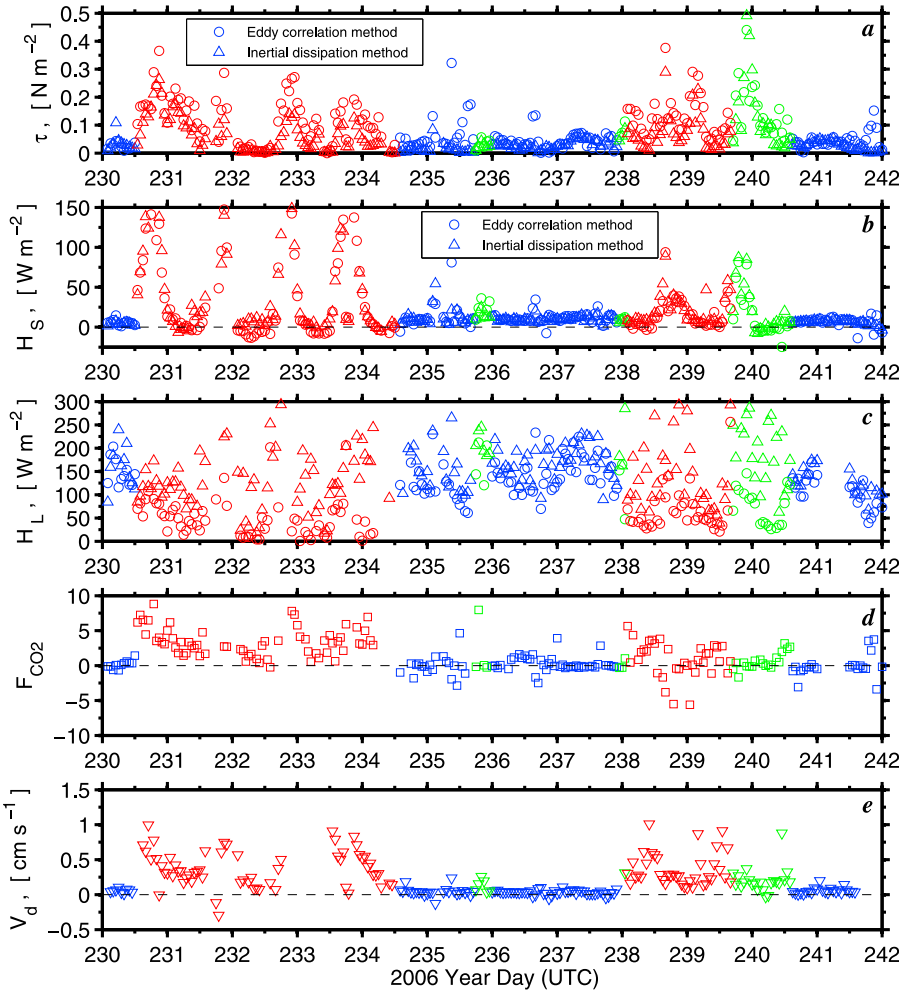

Figure 13. Same as Figure 10 but for data obtained during year days 230–242 (18–30 August 2006). The unit of measurement of CO_2 flux (Figure 13d) is μmol m s^{-1}.

[2002] and *Moriwaki and Kanda* [2004] for similar suburban areas of Chicago and Tokyo (in July), respectively. However, the magnitude of the CO_2 fluxes reported here as well as in other suburban areas is less than the CO_2 fluxes measured over a densely built-up urban center [*Grimmond et al.*, 2004; *Velasco et al.*, 2005, 2009; *Vogt et al.*, 2006], mainly because of higher vehicular traffic levels. One may expect that measurements in Houston downtown will lead to CO_2 fluxes similar that reported for other city centers.

[43] Ozone uptake to the surface was observed over water and over land (Figures 15b and 15c). However, ozone transfer over water (i.e., deposition to the water surface) and over land have a different nature and are described by different dependencies. The Houston Ship Channel surroundings are characterized by a typical American suburban surface built up by residential houses, one-story garages, flat commercial-industrial buildings, open green spaces with lawns, trees, shrubs, parking lots, and bare soil. The urban vegetation is an important ozone sink owing to efficient uptake of ozone by the leaf stomata. Also, the Houston urban core and the industrial complex along the Ship Channel and Galveston Bay (petrochemical facilities, power plants, etc.) are areas of emissions of NO_x, SO_2, and reactive hydrocarbons. Reaction of ozone with nitrogen monoxide, NO, emitted from sources along the industrial ship channel region as well the urban vegetation are likely to provide the main ozone sink for our inland measurement, rather than deposition to the surface. Satellite images of typical urban morphology representing commercial/industrial area, high-density residential area, and low-density residential area in the Houston area is given by *Lee et al.* [2011, Figure 3].

[44] Previous measurements show quite a range in observed ozone deposition velocity (14) over ocean water surfaces. *Ganzeveld et al.* [2009] recently summarized the ozone deposition velocities for ocean waters which range from 0.01 to 0.15 cm s^{-1} [*Ganzeveld et al.*, 2009, Table 1]. According to our data collected over the Gulf of Mexico, the averaged value of the ozone deposition velocity increases with wind speed, U, from ~0.02 cm s^{-1} at U = 1 m s^{-1} to 0.055 cm s^{-1} at U = 7 m s^{-1} (Figure 16b), and the median value of the deposition velocity is V_d = 0.035 cm s^{-1} (Table 1). The median downward ozone flux over the Gulf of Mexico was 14.89 μg m^{-2} s^{-1} (Table 1) with 1 h peak values reached up to 100 μg m^{-2} s^{-1} (Figure 16a). The median ozone concentration over the Gulf of Mexico during the experiment was 35.1 parts per billion by volume (ppbv) (ranged from 17.1 ppbv to 102.5 ppbv). Our data on the ozone

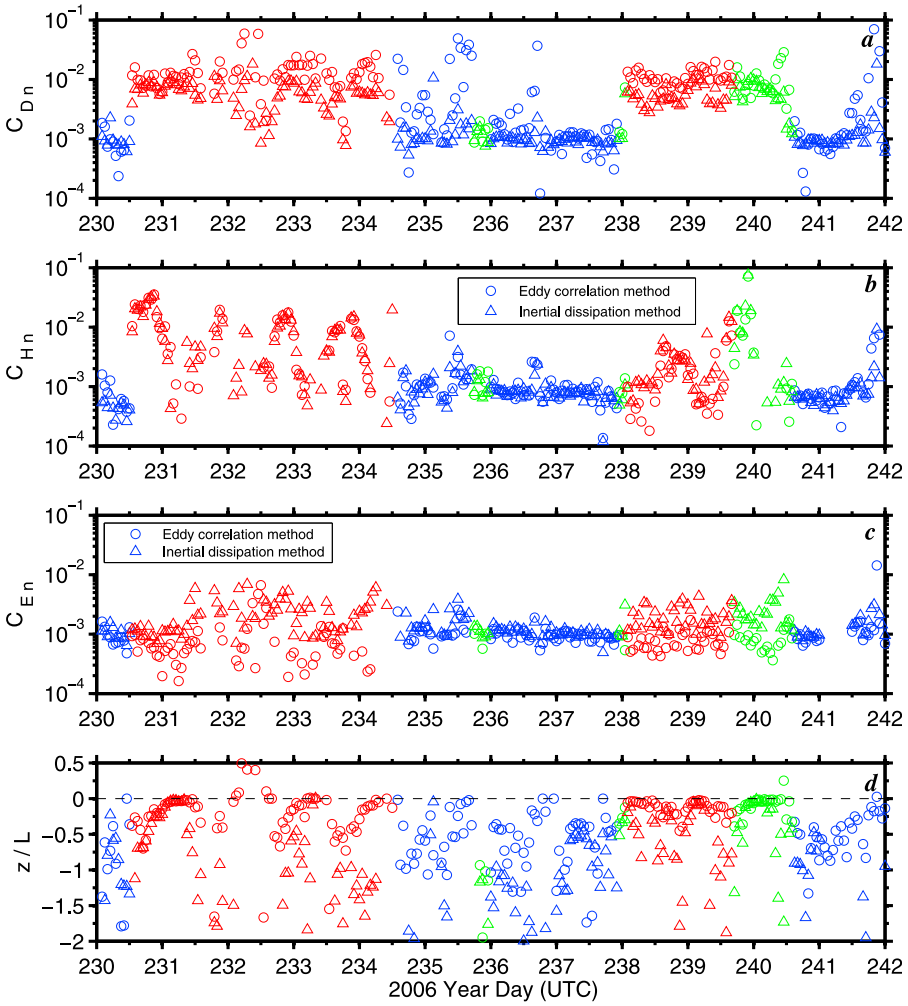

Figure 14. Same as Figure 11 but for data obtained during year days 230–242 (18–30 August 2006).

deposition velocity are in good agreement with the ozone flux measurements by *Lenschow et al.* [1982], *Kawa and Pearson* [1989], and *Whitehead et al.* [2010]. According to *Lenschow et al.* [1982, Table 1], the ozone deposition velocity is V_d = 0.05 cm s^{-1} for aircraft eddy correlation measurements over the waters of the Gulf of Mexico. *Kawa and Pearson* [1989] found an averaged value V_d = 0.026 cm s^{-1} (standard error ± 0.005 cm s^{-1}) measured by a low-flying aircraft off the Southern California coast in July and August 1985. *Whitehead et al.* [2010] recently reported an average value V_d = 0.0302 cm s^{-1} (standard error ± 0.0095 cm s^{-1}) observed over coastal seawaters during high tide at the Station Biologique de Roscoff, on the coast of Brittany, northwest France. *Galbally and Roy* [1980, Table 5] reported two values of the ozone deposition velocity measured in situ over the water surface at Aspendale Beach, Australia [see also *Chang et al.*, 2004, Figure 2], for calm weather V_d = 0.033 cm s^{-1}, which is close to our result, and V_d = 0.068 cm s^{-1} for wind speeds around 6 m s^{-1}, which is roughly twice the magnitude of our observations (see averaged value of V_d in Figure 16b for U = 6 m s^{-1}). *Gallagher et al.* [2001] reported a clear diurnal cycle of the ozone flux and the ozone deposition velocity on the basis of eddy correlation measurements made over coastal waters of the North Sea near Norfolk, UK. In their study, the mean values of V_d within each 1 h period range from 0.05 to 0.25 cm s^{-1} [*Gallagher et al.*, 2001, Figure 4] and the average measured ozone deposition velocity was found to be 0.105 cm s^{-1} [*Gallagher et al.*, 2001, Table 1]. This result is higher compared to the value of V_d mentioned earlier, and is likely to be associated with local conditions in terms of turbulence and biogeochemistry.

[45] The range of ozone deposition velocities reported for over water measurements is much smaller than continental deposition velocities. For example, *Lenschow et al.* [1982, Table 1] found $V_d \approx$ 1 cm s^{-1} measured over pine forests near the Gulf of Mexico coast and *Fan et al.* [1990] reported the mean ozone deposition velocity 0.26 cm s^{-1} in the night and 1.8 cm s^{-1} in the day with maximum values up to 2.7 cm s^{-1} [*Fan et al.*, 1990, Figure 10] for data collected at a level 10 m above the canopy of the Amazon forest. The averaged ozone deposition velocities, V_d, based on our data collected inland over different locations range from 0.24 to 1.42 cm s^{-1} (see Table 1), and daytime 1 h peak values reached up to 4 cm s^{-1} (Figure 10e). These values match other estimations of V_d obtained over land. The averaged

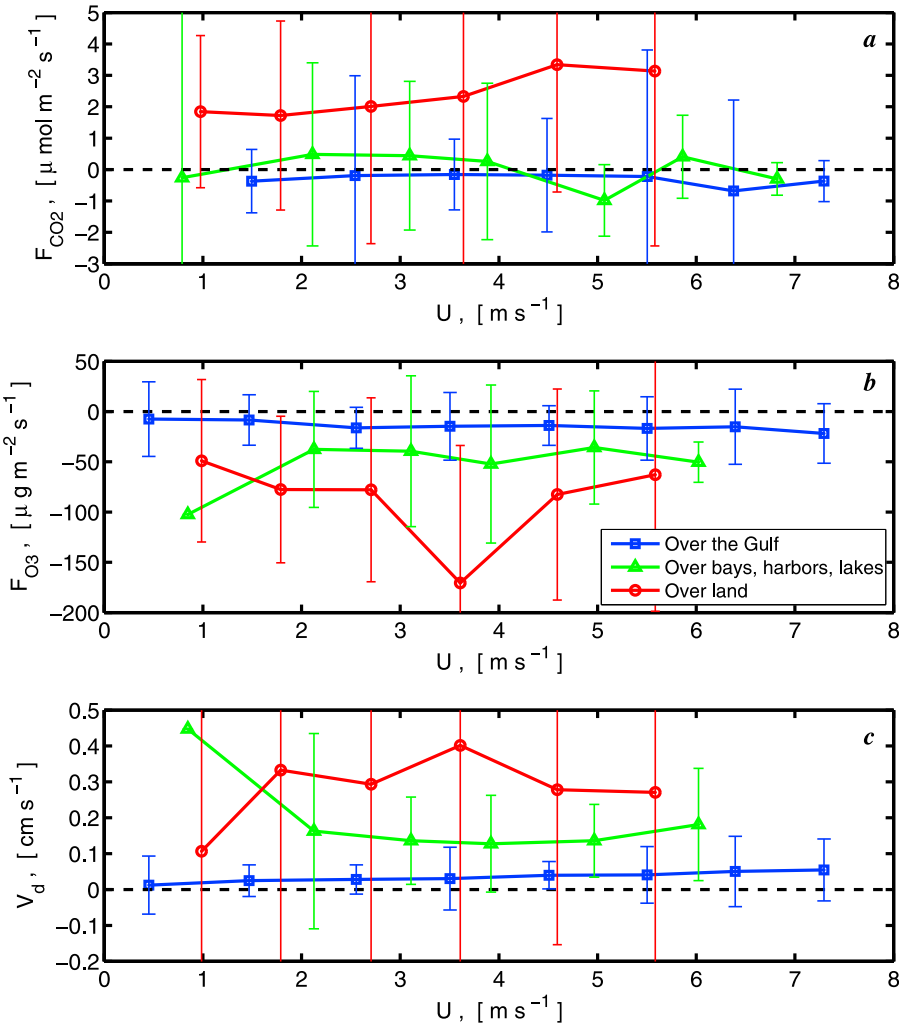

Figure 15. Plots of the bin-averaged data of (a) carbon dioxide turbulent flux (eddy covariance), (b) ozone turbulent flux (eddy covariance), and (c) ozone deposition velocity (equation (14)) versus wind speed. Measurements made over the Gulf of Mexico (blue squares); over the bays, lakes, and near coastal harbor areas (green triangles); and over land (red circles) are plotted separately. Error bars show the standard deviation of the binned data points. Width of bins is 1 m s^{-1}.

Table 1. Averaged Median Values of Carbon Dioxide and Ozone Turbulent Fluxes and the Ozone Deposition Velocity Measured at Different Locations[a]

Location Code	Location Name	CO_2 Turbulent Flux (μmol m^{-2} s^{-1})	O_3 Turbulent Flux (μg m^{-2} s^{-1})	O_3 Deposition Velocity (cm s^{-1})
1	Gulf of Mexico	−0.2368	−14.8909	0.0354
2	Galveston Bay	0.1706	−45.3843	0.1412
3	Port of Galveston	2.9426	−168.852	0.3352
4	Sabine River and Lake	−1.7327	−32.7387	0.0788
5	Beaumont	1.7467	−122.131	0.5096
6	Barbour's Cut	1.6198	−65.985	0.2418
7	Houston Ship Channel	2.7978	−83.2331	1.4228
8	Freeport Harbor	−2.4589	NA[b]	NA[b]
9	Matagorda Bay	−0.0652	−58.8935	0.1113
10	Jacintoport	2.5427	NA[b]	NA[b]

[a]Carbon dioxide and ozone turbulent fluxes are given as eddy covariance measurements. See equation (14). See also details in section 4.
[b]NA, data not available.

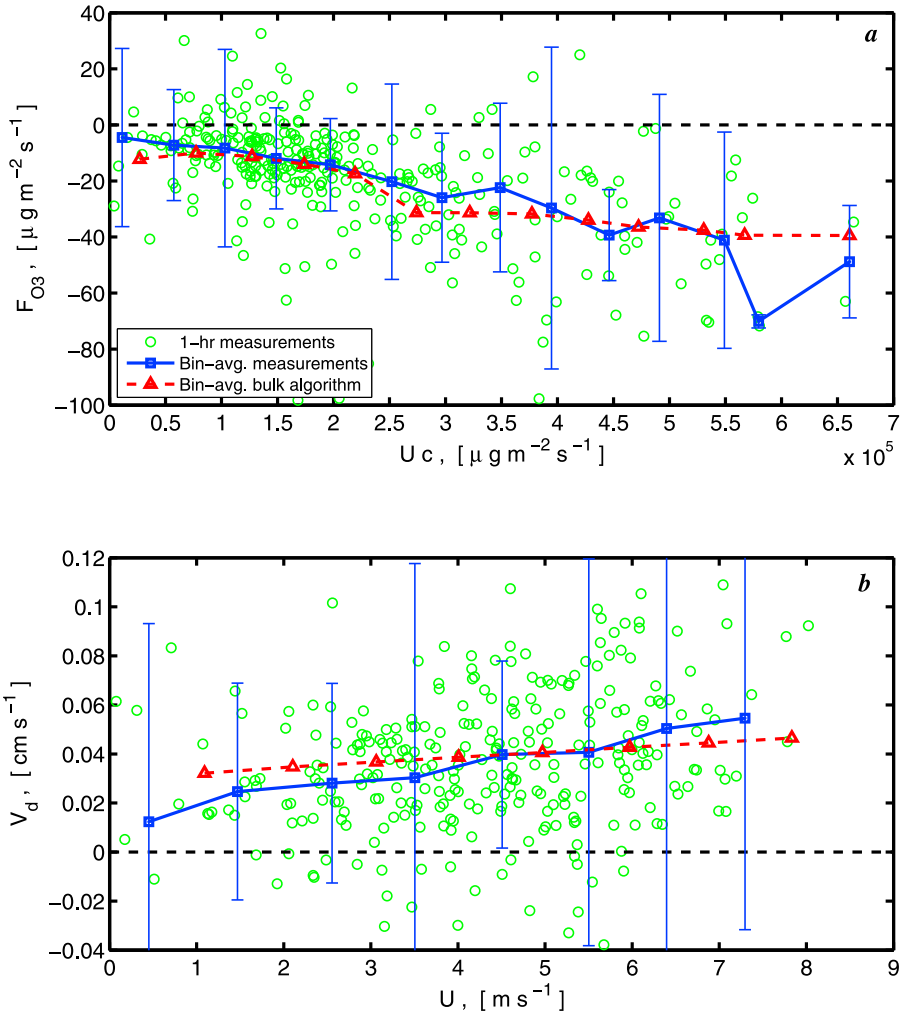

Figure 16. Plots of the bin-averaged (blue squares) and individual 1 h data (green circles) of (a) ozone turbulent flux (eddy covariance) versus the product of wind speed by mean ozone concentration and (b) ozone deposition velocity (equation (14)) versus the wind speed for over the Gulf of Mexico measurements. The red triangles indicate the ozone version of the NOAA COARE gas transfer model [*Fairall et al.*, 2007]. Error bars show the standard deviation of the binned data points. Width of bins is 5×10^5 μg m^{-2} s^{-1} (Figure 16a) and 1 m s^{-1} (Figure 16b).

ozone turbulent flux measured inland range from ~66 to 169 μg m^{-2} s^{-1} (Table 1).

[46] As mentioned earlier, the study of ozone transport is one of the primary focus areas of the TexAQS 2006 field campaign. Several high-ozone-event days in the Houston area were reported by the Texas Commission on Environmental Quality during the experimental period, and these incidents were confirmed by measurements aboard the ship; for example, during 4 August (YD 216–217 UTC), 16–18 August (YD 228–231 UTC), 31 August to 2 September (243–246 UTC), and 7 September 2006 (YD 250–251 UTC). For example, the highest 1 h average ozone concentration of 169 ppbv was observed on 1 September 2006 as the ship was crossing the Galveston Bay [e.g., *Tucker et al.*, 2010, Figures 11 and 12]. Our data (e.g., Figures 10e and 13e) do not show obvious correlation between the near-surface ozone deposition velocity and the high ozone events.

[47] However, we do find correlation between ozone turbulent flux and the governing near-surface parameters for over water measurements. Figure 16 shows bin-averaged dependencies (Figure 16a) of the ozone turbulent flux versus the product of wind speed and mean ozone concentration, and (Figure 16b) the ozone deposition velocity (14) versus the wind speed.

[48] Our data obtained over water suggest that the ozone flux increases almost linearly with increasing $U \cdot c$ with a slope is close to 10^{-4} (Figure 16a). The wind speed dependence of the ozone deposition velocity for over water measurements in Figure 16b is fairly similar to model results by *Fairall et al.* [2007, Figure 3]. The bin-averaged experimental data in Figure 16 agree well with the ozone version of the NOAA COARE gas transfer model [*Fairall et al.*, 2000, 2007; *Hare et al.*, 2004]. The model was run with an ozone waterside reaction rate of 10^3 s^{-1}, a Schmidt number Sc = 500, and the Henry law constant H = 3. The ozone model uses temperature-dependent solubility and Schmidt numbers. The individual 1 h–averaged data based on the median values are also shown in Figure 16 as

green circles. These points give an estimate of the available data at all levels and demonstrate the typical scatter of the data.

7. Conclusions

[49] The TexAQS/GoMACCS ship-based field campaign in the summer of 2006 was a unique study of surface turbulent fluxes of momentum, sensible and latent heat, and trace gases (carbon dioxide and ozone) in the coastal waters of the Gulf of Mexico, nearby bay/harbor areas of the southeastern Texas, and far inland along ship channels and rivers (up to 12 km from Houston downtown). We compared turbulent fluxes measured over the sea surface and over land; that is, in urban and suburban areas which are rough aerodynamic surfaces.

[50] The turbulent data collected aboard the R/V *Ronald H. Brown* have been broken into three sampling categories: (1) open sea locations; (2) bays, lakes, and near coastal harbor areas; and (3) urban/suburban inland locations. Our analysis indicates that the COARE bulk flux algorithm [*Fairall et al.*, 2003] reasonably describes the air-sea turbulent fluxes (1)–(3) measured over the coastal waters of the Gulf of Mexico, although the bulk algorithm overestimates the sensible and latent heat flux by ~10% (see Figures 4 and 5). This discrepancy may be associated with a possible coastal influence on the turbulent fluxes. However, data collected during the TexAQS 2006 field campaign show that the air–sea fluxes measured close to shore are much less affected by coastal effects as compared to the NEAQS 2004 results [*Fairall et al.*, 2006]. This implies that coastal effects have a smaller impact on air-sea interaction in the coastal zone when convective conditions are observed both over sea and land during day and night and in the absence of ocean swell. These conditions are essentially different compared to the shallow, stable boundary layers over the cool waters of the Gulf of Maine between Cape Cod and Nova Scotia, observed in summer 2004 during NEAQS [*Angevine et al.*, 2006; *Fairall et al.*, 2006].

[51] We found a sharp change in the momentum flux and the drag coefficient for sea-land transitions, obviously due to the change in surface characteristics. The neutral drag coefficient over aerodynamically rough urban areas increases dramatically and can be as much as a factor of 20 larger than over a relatively smooth sea surface (see Figures 8a and 14a). However, similar effects were not observed for the sensible and latent heat fluxes. The neutral Stanton and Dalton numbers do not change significantly for inland measurements as compared to the measurements made over the Gulf of Mexico (Figures 8b and 8c). However, the data for C_{Hn} and C_{En} presented in Figures 8b and 8c are restricted only to night conditions when the measured water temperature is close to the land footprint temperature. The increased drag coefficient over the urban surfaces is probably due to the effect of pressure drag induced by urban structures. These urban roughness elements influence the wind profile and are presumed to enhance the momentum transfer through pressure terms in the Navier-Stokes equations, whereas pressure transport does not affect the sensible and latent heat flux. According to our study, the turbulent transfer over different harbors/bays areas is mainly an intermediate case between over-sea and overland locations.

[52] Besides the traditional air-sea fluxes of the momentum, sensible and latent heat, we examined carbon dioxide and ozone turbulent transfer. The turbulent fluxes of carbon dioxide reported here fit well into the general scheme of carbon dioxide measurements. The CO_2 flux was mostly negative (uptake by the surface) over the Gulf of Mexico and some bays but becomes positive (release to the air) when measurement were made inland. The average value of the CO_2 turbulent flux over the Gulf of Mexico was -7.47 mol m^{-2} yr^{-1} which was consistent with the results obtained earlier during GasEx-1998. The average CO_2 flux measured over a suburban area of Houston along the Ship Channel was about 2.8 μmol m^{-2} s^{-1} with peak values of 15 μmol m^{-2} s^{-1}, which is in good agreement with other suburban studies.

[53] Our data suggest that the surface generally acts as a sink for ozone for both overland and over-sea surfaces. On average, the ozone deposition velocity (14) ranges from 0.035 cm s^{-1} for measurements over waters of the Gulf of Mexico to 0.24–1.42 cm s^{-1} over different inland locations (Table 1). Both CO_2 and O_3 turbulent fluxes over land were observed to be larger in magnitude and have higher variability compared to the over water measurements.

[54] **Acknowledgments.** The authors thank all of the participants in GoMACCS/TexAQS 2006 who aided in the operation of these instruments and in the collection of data. Special thanks go to David Welsh, William Otto, Daniel Wolfe, Sergio Pezoa, and the dedicated officers and crew of the NOAA R/V *Ronald H. Brown*. This work was supported by the NOAA Health of the Atmosphere Program and by the NOAA Climate Program Office's Global Carbon Cycle Program.

References

Angevine, W. M., J. E. Hare, C. W. Fairall, D. E. Wolfe, R. J. Hill, W. A. Brewer, and A. B. White (2006), Structure and formation of the highly stable marine boundary layer over the Gulf of Maine, *J. Geophys. Res.*, *111*, D23S22, doi:10.1029/2006JD007465.

Bariteau, L., D. Helmig, C. W. Fairall, J. E. Hare, J. Hueber, and E. K. Lang (2010), Determination of oceanic ozone deposition by ship-borne eddy covariance flux measurements, *Atmos. Meas. Tech.*, *3*, 441–455, doi:10.5194/amt-3-441-2010.

Bates, T. S., et al. (2008), Boundary layer aerosol chemistry during TexAQS/GoMACCS 2006: Insights into aerosol sources and transformation processes, *J. Geophys. Res.*, *113*, D00F01, doi:10.1029/2008JD010023.

Chang, W., B. G. Heikes, and M. Lee (2004), Ozone deposition to the sea surface: Chemical enhancement and wind speed dependence, *Atmos. Environ.*, *38*, 1053–1059, doi:10.1016/j.atmosenv.2003.10.050.

Christen, A., R. Vogt, and M. W. Rotach (2009), The budget of turbulent kinetic energy in the urban roughness sublayer, *Boundary Layer Meteorol.*, *131*, 193–222, doi:10.1007/s10546-009-9359-5.

Coceal, O., and S. E. Belcher (2004), A canopy model of mean winds through urban areas, *Q. J. R. Meteorol. Soc.*, *130*, 1349–1372, doi:10.1256/qj.03.40.

Day, B. M., B. Rappenglück, C. B. Clements, S. C. Tucker, and W. A. Brewer (2010), Nocturnal boundary layer characteristics and land breeze development in Houston, Texas, during TexAQS II, *Atmos. Environ.*, *44*, 4014–4023, doi:10.1016/j.atmosenv.2009.01.031.

Edson, J. B., J. E. Hare, and C. W. Fairall (1998), Direct covariance flux estimates from moving platforms at sea, *J. Atmos. Oceanic Technol.*, *15*, 547–562, doi:10.1175/1520-0426(1998)015<0547:DCFEFM>2.0.CO;2.

Fairall, C. W., E. F. Bradley, J. S. Godfrey, G. A. Wick, J. B. Edson, and G. S. Young (1996a), Cool skin and warm layer effects on the sea surface temperature, *J. Geophys. Res.*, *101*, 1295–1308, doi:10.1029/95JC03190.

Fairall, C. W., E. F. Bradley, D. P. Rogers, J. B. Edson, and G. S. Young (1996b), Bulk parameterization of air-sea fluxes for Tropical Ocean-Global Atmosphere Coupled-Ocean Atmosphere Response Experiment, *J. Geophys. Res.*, *101*, 3747–3764, doi:10.1029/95JC03205.

Fairall, C. W., A. B. White, J. B. Edson, and J. E. Hare (1997), Integrated shipboard measurements of the marine boundary layer, *J. Atmos. Oce-*

anic Technol., *14*, 338–359, doi:10.1175/1520-0426(1997)014<0338:ISMOTM>2.0.CO;2.

Fairall, C. W., J. E. Hare, J. B. Edson, and W. R. McGillis (2000), Measurement and parameterization of the air–sea gas transfer, *Boundary Layer Meteorol.*, *96*, 63–106, doi:10.1023/A:1002662826020.

Fairall, C. W., E. F. Bradley, J. E. Hare, A. A. Grachev, and J. B. Edson (2003), Bulk parameterization of air-sea fluxes: Updates and verification for the COARE algorithm, *J. Clim.*, *16*, 571–591, doi:10.1175/1520-0442(2003)016<0571:BPOASF>2.0.CO;2.

Fairall, C. W., L. Bariteau, A. A. Grachev, R. J. Hill, D. E. Wolfe, W. A. Brewer, S. C. Tucker, J. E. Hare, and W. M. Angevine (2006), Turbulent bulk transfer coefficients and ozone deposition velocity in the International Consortium for Atmospheric Research into Transport and Transformation, *J. Geophys. Res.*, *111*, D23S20, doi:10.1029/2006JD007597.

Fairall, C. W., D. Helmig, L. Ganzeveld, and J. Hare (2007), Water-side turbulence enhancement of ozone deposition to the ocean, *Atmos. Chem. Phys.*, *7*, 443–451, doi:10.5194/acp-7-443-2007.

Fan, S.-M., S. C. Wofsy, P. S. Bakwin, D. J. Jacob, and D. R. Fitzjarrald (1990), Atmosphere-biosphere exchange of CO_2 and O_3 in the central Amazon forest, *J. Geophys. Res.*, *95*, 16,851–16,864, doi:10.1029/JD095iD10p16851.

Galbally, I. E., and C. R. Roy (1980), Destruction of ozone at the Earth's surface, *Q. J. R. Meteorol. Soc.*, *106*, 599–620, doi:10.1002/qj.49710644915.

Gallagher, M. W., K. M. Beswick, and H. Coe (2001), Ozone deposition to coastal waters, *Q. J. R. Meteorol. Soc.*, *127*, 539–558, doi:10.1002/qj.49712757215.

Ganzeveld, L., D. Helmig, C. W. Fairall, J. Hare, and A. Pozzer (2009), Atmosphere-ocean ozone exchange: A global modeling study of biogeochemical, atmospheric, and waterside turbulence dependencies, *Global Biogeochem. Cycles*, *23*, GB4021, doi:10.1029/2008GB003301.

Grachev, A. A., C. W. Fairall, and S. E. Larsen (1998), On the determination of the neutral drag coefficient in the convective boundary layer, *Boundary Layer Meteorol.*, *86*, 257–278, doi:10.1023/A:1000617300732.

Grimmond, C. S. B., and T. R. Oke (1999), Aerodynamic properties of urban areas derived from analysis of surface form, *J. Appl. Meteorol.*, *38*, 1262–1292, doi:10.1175/1520-0450(1999)038<1262:APOUAD>2.0.CO;2.

Grimmond, C. S. B., T. S. King, M. Roth, and T. R. Oke (1998), Aerodynamic roughness of urban areas derived from wind observations, *Boundary Layer Meteorol.*, *89*, 1–24, doi:10.1023/A:1001525622213.

Grimmond, C. S. B., T. S. King, F. D. Cropley, D. J. Nowak, and C. Souch (2002), Local-scale fluxes of carbon dioxide in urban environments: Methodological challenges and results from Chicago, *Environ. Pollut.*, *116*, suppl. 1, S243–S254, doi:10.1016/S0269-7491(01)00256-1.

Grimmond, C. S. B., J. A. Salmond, T. R. Oke, B. Offerle, and A. Lemonsu (2004), Flux and turbulence measurements at a densely built-up site in Marseille: Heat, mass (water and carbon dioxide), and momentum, *J. Geophys. Res.*, *109*, D24101, doi:10.1029/2004JD004936.

Hare, J. E., C. W. Fairall, W. R. McGillis, J. B. Edson, B. Ward, and R. Wanninkhof (2004), Evaluation of the National Oceanic and Atmospheric Administration/Coupled-Ocean Atmospheric Response Experiment (NOAA/COARE) air-sea gas transfer parameterization using GasEx data, *J. Geophys. Res.*, *109*, C08S11, doi:10.1029/2003JC001831.

Kastner-Klein, P., and M. W. Rotach (2004), Mean flow and turbulence characteristics in an urban roughness sublayer, *Boundary Layer Meteorol.*, *111*, 55–84, doi:10.1023/B:BOUN.0000010994.32240.b1.

Kawa, S. R., and R. Pearson Jr. (1989), Ozone budgets from the dynamics and chemistry of Marine Stratocumulus Experiment, *J. Geophys. Res.*, *94*, 9809–9817, doi:10.1029/JD094iD07p09809.

Klipp, C. (2007), Wind direction dependence of atmospheric boundary layer turbulence parameters in the urban roughness sublayer, *J. Appl. Meteorol. Climatol.*, *46*, 2086–2097, doi:10.1175/2006JAMC1298.1.

Langford, A. O., S. C. Tucker, C. J. Senff, R. M. Banta, W. A. Brewer, R. J. Alvarez II, R. M. Hardesty, B. M. Lerner, and E. J. Williams (2010), Convective venting and surface ozone in Houston during TexAQS 2006, *J. Geophys. Res.*, *115*, D16305, doi:10.1029/2009JD013301.

Lee, S.-H., S.-W. Kim, W. M. Angevine, L. Bianco, S. A. McKeen, C. J. Senff, M. Trainer, S. C. Tucker, and R. J. Zamora (2011), Evaluation of urban surface parameterizations in the WRF model using measurements during the Texas Air Quality Study 2006 field campaign, *Atmos. Chem. Phys.*, *11*, 2127–2143, doi:10.5194/acp-11-2127-2011.

Lenschow, D. H., R. Pearson Jr., and B. B. Stankov (1982), Measurements of ozone vertical flux to ocean and forest, *J. Geophys. Res.*, *87*, 8833–8837, doi:10.1029/JC087iC11p08833.

Leuning, R. (2007), The correct form of the Webb, Pearman and Leuning equation for eddy fluxes of trace gases in steady and non-steady state, horizontally homogeneous flows, *Boundary Layer Meteorol.*, *123*, 263–267, doi:10.1007/s10546-006-9138-5.

Leuning, R., and B. J. Legg (1982), Comment on "The influence of water vapor fluctuations on turbulent fluxes" by R. Brook, *Boundary Layer Meteorol.*, *23*, 255–258, doi:10.1007/BF00123302.

Mahrt, L., D. Vickers, P. Frederickson, K. Davidson, and A.-S. Smedman (2003), Sea-surface aerodynamic roughness, *J. Geophys. Res.*, *108*(C6), 3171, doi:10.1029/2002JC001383.

McGillis, W. R., J. B. Edson, J. E. Hare, and C. W. Fairall (2001a), Direct covariance air–sea CO_2 fluxes, *J. Geophys. Res.*, *106*, 16,729–16,745, doi:10.1029/2000JC000506.

McGillis, W. R., J. B. Edson, J. D. Ware, J. W. H. Dacey, J. E. Hare, C. W. Fairall, and R. Wanninkhof (2001b), Carbon dioxide flux techniques performed during GasEx-98, *Mar. Chem.*, *75*, 267–280, doi:10.1016/S0304-4203(01)00042-1.

McGillis, W. R., et al. (2004), Air-sea CO_2 exchange in the equatorial Pacific, *J. Geophys. Res.*, *109*, C08S02, doi:10.1029/2003JC002256.

Monin, A. S., and A. M. Obukhov (1954), Basic laws of turbulent mixing in the surface layer of the atmosphere, *Tr. Akad. Nauk SSSR Geofiz. Inst.*, *24*, 163–187.

Moriwaki, R., and M. Kanda (2004), Seasonal and diurnal fluxes of radiation, heat, water vapor, and carbon dioxide over a suburban area, *J. Appl. Meteorol.*, *43*, 1700–1710, doi:10.1175/JAM2153.1.

Obukhov, A. M. (1946), Turbulence in an atmosphere with a non-uniform temperature [in Russian], *Tr. Inst. Teoret. Geofiz. Akad. Nauk. SSSR*, *1*, 95–115. [*Boundary Layer Meteorol., Engl. Transl.*, *2*, 7–29, 1971.]

Raupach, M. R. (1992), Drag and drag partition on rough surfaces, *Boundary Layer Meteorol.*, *60*, 375–395, doi:10.1007/BF00155203.

Raupach, M. R., R. A. Antonia, and S. Rajagopalan (1991), Rough wall turbulent boundary layers, *Appl. Mech. Rev.*, *44*, 1–25, doi:10.1115/1.3119492.

Rotach, M. W. (1993), Turbulence close to a rough urban surface, part I: Reynolds stress, *Boundary Layer Meteorol.*, *65*, 1–28, doi:10.1007/BF00708816.

Rotach, M. W. (1999), On the influence of the urban roughness sublayer on turbulence and dispersion, *Atmos. Environ.*, *33*, 4001–4008, doi:10.1016/S1352-2310(99)00141-7.

Roth, M. (2000), Review of atmospheric turbulence over cities, *Q. J. R. Meteorol. Soc.*, *126*, 941–990, doi:10.1256/smsqj.56408.

Sabins, F. F. (1987), *Remote Sensing: Principles and Interpretation*, W. H. Freeman, New York.

Shao, Y., and Y. Yang (2005), A scheme for drag partition over rough surfaces, *Atmos. Environ.*, *39*, 7351–7361, doi:10.1016/j.atmosenv.2005.09.014.

Tucker, S. C., R. M. Banta, A. O. Langford, C. J. Senff, W. A. Brewer, E. J. Williams, B. M. Lerner, H. D. Osthoff, and R. M. Hardesty (2010), Relationships of coastal nocturnal boundary layer winds and turbulence to Houston ozone concentrations during TexAQS 2006, *J. Geophys. Res.*, *115*, D10304, doi:10.1029/2009JD013169.

Velasco, E., S. Pressley, E. Allwine, H. Westberg, and B. Lamb (2005), Measurements of CO_2 fluxes from the Mexico City urban landscape, *Atmos. Environ.*, *39*, 7433–7446, doi:10.1016/j.atmosenv.2005.08.038.

Velasco, E., et al. (2009), Eddy covariance flux measurements of pollutant gases in urban Mexico City, *Atmos. Chem. Phys.*, *9*, 7325–7342, doi:10.5194/acp-9-7325-2009.

Vogt, R., A. Christen, M. W. Rotach, M. Roth, and A. N. V. Satyanarayana (2006), Temporal dynamics of CO_2 fluxes and profiles over a central European city, *Theor. Appl. Climatol.*, *84*, 117–126, doi:10.1007/s00704-005-0149-9.

Webb, E. K. (1982), On the correction of flux measurements for effects of heat and water vapour transfer, *Boundary Layer Meteorol.*, *23*, 251–254, doi:10.1007/BF00123301.

Webb, E. K., G. I. Pearman, and R. Leuning (1980), Correction of flux measurements for density effects due to heat and water vapour transfer, *Q. J. R. Meteorol. Soc.*, *106*, 85–100, doi:10.1002/qj.49710644707.

Whitehead, J. D., G. McFiggans, M. W. Gallagher, and M. J. Flynn (2010), Simultaneous coastal measurements of ozone deposition fluxes and iodine-mediated particle emission fluxes with subsequent CCN formation, *Atmos. Chem. Phys.*, *10*, 255–266, doi:10.5194/acp-10-255-2010.

L. Bariteau, C. W. Fairall, A. A. Grachev, and J. E. Hare, NOAA Earth System Research Laboratory, 325 Broadway, R/PSD3, Boulder, CO 80305-3337, USA. (andrey.grachev@noaa.gov)

D. Helmig, J. Hueber, and E. K. Lang, Institute of Alpine and Arctic Research, University of Colorado at Boulder, Boulder, CO 80309, USA.